Mechanical development of an automated guided vehicle

Matthieu LAMY

AKÉO + PLUS
SMART TECHNOLOGIES & ROBOTICS

Master of Science Thesis MMK 2016:153 MKN 171
KTH Industrial Engineering and Management
Machine Design
SE-100 44 STOCKHOLM

KTH Industriell teknik och management

Examensarbete MMK 2016:153 MKN 171

Mekanisk utveckling av ett automatiskt styrt fordon

Matthieu LAMY

Godkänt	Examinator	Handledare
2016-10-10	Ulf Sellgren	Ulf Sellgren
	Uppdragsgivare	Kontaktperson
	Akéo Plus	Valentin Leduc

Sammanfattning

Automatiskt styrda fordon, AGV, används allt mer i fabriker för att ge en smart och anpassningsbar materialhantering baseratdpå lokaliseringsteknik. För att möjliggöra användande av visions- och vägspårningsteknologi till dess rätta potential för automatiskt styrda fordon behövs ett mekaniskt system som kan röra sig på små ytor.

Syftet med studien har varit att utveckla den mekaniska strukturen till en AGV. Strukturen består av ett chassi och mecanumhjul. För att uppfylla behovet, måste fordonet kunna bära stora laster samtidigt som det ska vara kompakt. Det krävdes även att den skulle vara billig för att vara konkurrenskraftig på marknaden.

Beräkningsmodeller har tagits fram för att möjliggöra utformning av mecanumhjulen. Den hjul- och chassiutformning som tagits fram uppfyller krav som löser problem i föregående utformningar. Prototypen har dock ej blivit fullt testad på grund av tillverkningsproblem av rullarna.

Studien har givit en stark bas för utformning av AGV och pekar ut vanliga problem relaterade till utformandet av holonomiska fordon. Lösningarna som presenterats i denna studie behöver testas för att validera utformningen.

Nyckelord: *AGV, Holonomiska fordon, Mecanumhjul, Mekanisk utveckling*

KTH Industrial Engineering and Management

Master of Science Thesis MMK 2016:153 MKN 171

Mechanical development of an automated guided vehicle

Matthieu LAMY

Approved	Examiner	Supervisor
2016-10-10	Ulf Sellgren	Ulf Sellgren
	Commissioner	Contact person
	Akéo Plus	Valentin Leduc

Abstract

Automated guided vehicles (AGV) are more and more used in factories to provide a smart and adaptable material handling based on localization technologies. To use vision and path finding technologies at their full potential in these vehicles, a mechanical system able to move within a small space is required.

The purpose of this study was to develop the mechanical structure of an AGV. The structure is composed of a chassis and mecanum wheels. To satisfy the needs, the vehicle had to be able to carry heavy loads while being compact. It also had to be cheap to be competitive on the market.

Calculation models were developed to design mecanum wheels. From these models, the structure of the vehicle has been designed. The obtained solution fulfils requirements and solves some problems encountered by the previous design of the vehicle. However the prototype haven't be fully tested due to manufacturing problems on rollers.

This study offers a strong basis to design an AGV and points out common problems related to the design of a holonomic vehicle. Furthermore, some of the solutions proposed in this study need to be tested for validation.

Keywords: *AGV, Holonomic vehicle, Mecanum wheel, Mechanical development*

FOREWORD

I would like to thank my thesis supervisor at KTH, Dr. Ulf Sellgren and my thesis supervisor at Arts et Métiers Paristech, Dr. Antoine Dazin. Their guidance and their trust have helped me to complete this thesis.

I also would like to thank my industrial supervisor Valentin Leduc for his support and his enthusiasm. His invaluable advices have helped me to overcome difficulties.

Special thanks to Benoit Maréchal and Pascal Grenet who have participated to brainstorming meetings. They have a wide experience in mechanical systems and standard components and I am thankful that they have shared it with me.

Matthieu Lamy

Stockholm, July 2016

NOMENCLATURE

Notations

Symbol	Description
α	Angle to position the contact point between floor and rollers (rad)
D_{axes}	Diameter of rollers' axes (m)
Db	Outer diameter of bushing flanges (m)
dr	Diameter of rollers depending on α (m)
Dr	Maximum radius of rollers (m)
Ds	Shaft diameter in the considered section (m)
E_c	Young's modulus of concrete (Pa)
E_p	Young's modulus of polyurethane 95A (Pa)
Ff	Friction force between the floor and a wheel (N)
Fr	Reaction force of the floor (N)
F_{rs}	Minimum pre-tensioning force of screws (N)
Frb	Preloading force of bearings (N)
Ft	Traction force of one wheel of the vehicle (N)
g	Gravity constant (m/s²)
L	Distance between attachment points of rollers (m)
Lb	Length of bushings (m)
$Ls1$	Distance between the back rim and the first bearing (m)
$Ls2$	Distance between the two bearings (m)
Lw	Distance between the contact point of the wheel on the floor and the fastening points on the support frame (m)
$\mu_{al,s}$	Friction coefficient between aluminum and steel (-)
μf	Coefficient of friction between polyurethane 95A and concrete (-)
$M_{b,y}$	Bending torque on the shaft in y direction (Nm)
$M_{b,z}$	Bending torque on the shaft in z direction (Nm)
Ml	Maximum mass of transported loads (kg)
M_t	Torsional torque on the shaft (Nm)
Mv	Mass of the vehicle (kg)
v_c	Poisson's ratio of concrete (-)
v_p	Poisson's ratio of polyurethane 95A (-)
N	Normal force in the considered section of the shaft (N)
P_0	Hertzian pressure (Pa)

ρ	Curvature radius of the ellipsoid (m)
Rc	Curvature radius of rollers (m)
Rw	Wheel radius (m)
σ	Normal stresses in a section of the shaft (Pa)
$\sigma_{t,max}$	Maximum shearing stress on the contact between floor and rollers due to friction (Pa)
$\sigma_{vm,s}$	Von Mises stresses in the shaft (Pa)
Sf	Safety factor (-)
S_{rs}	Area of sheared surface of rollers' axes (m²)
τ	Shearing stresses in a section of the shaft (Pa)
$\tau_{rs,max}$	Maximum shearing stress in rollers' axes (Pa)
Tm	Maximum torque provided by the motor (Nm)
x	Position of curvature center of ellipsoid in x3 direction (m)
y	Position of curvature center of ellipsoid in y3 direction (m)
Y	Bearing constant (-)

Abbreviations

AGV	Automated Guided Vehicle
CAD	Computer Aided Design
FEA	Finite Element Analysis
PMMA	Polymethyl methacrylate
VDI	Verein Deutscher Ingenieure (Association of German engineers)

TABLE OF CONTENTS

1 INTRODUCTION

This chapter describes the structure of the project. It includes the background, the purpose, the limitations and the methods used in this thesis. This chapter is also aimed at giving an insight of the surrounding environment of the project.

1.1 Background

This part describes the environment of the study, including the company where the study was performed.

Presentation of company

This master thesis has been performed at Akéo Plus, a young and dynamic company located in Château-Gaillard (France). When the company was created in 2006, it developed algorithms for sensors. Customers' needs quickly brought Akéo Plus to integrate sensors with its own algorithms in articulated robots. Nowadays, the company is still providing technical support by integrating its solutions into customers' products but it's also designing its own products. One example of these products, named Akeobot, is presented in Figure 1. Akeobot is a collaborative robot recently developed by the company.

Figure 1. Collaborative robot: Akeobot.

The goal of Akéo Plus is to be a leading actor on the market of smart machines. To reach this goal, the strategy of the company is based on two key points. The first point is to increase the productivity of factories by improving the value of workers and so by reducing the number of repetitive and valueless tasks they realize. The second point is to increase the flexibility of factories by making products which enable customers to quickly modify their production.

Industrial context

Automation of manufacturing processes has become more and more important. The increasing need of automated systems can be explained by the complexity of processes involved as well as the complexity of products and the number of steps needed to make them. For example, the manufacturing of integrated circuits can imply more than 100 steps (Internsil group, 2010). Furthermore, the total manufacturing process may include several uses of the same tool for different processing steps and so it requires a high level of logistic for material handling. In order to retain productivity and efficiency of factories, automation of material handling has become a key aspect of automation for many companies.

Driverless material handling systems called Automated Guided Vehicles (AGVs) have been introduced in car industry in the 1950s. The first AGV was a tow truck which was able to follow

a track made of a wire (Egemin automation, 2001). Since the introduction of this AGV, a lot of new guidance technologies have appeared. With the development of these technologies, the need of mechanical systems which are able to move in small spaces and carry heavy loads has increased as well.

Automated Guided Vehicle

In order to respond to customers' needs in terms of automation and to follow its strategy of developing smarter factories, Akéo Plus is currently developing a new AGV. The vehicle will be able to move autonomously within the workshop based on localisation technology using laser sensors. The two sensors located on opposite corners of AGV provide localisation informations and are also used as safety system which makes the vehicle collaborative.

The company wants to develop a vehicle that would be set in the workshop without any major modification of the factory. So the AGV must be compact and use holonomic displacements to reduce the space needed and ideally to move in paths already existing for operators.

1.2 Purpose

The purpose of this study was to realise the development of mecanum wheels for the AGV as well as the chassis which carries wheels, batteries and the payload. The design had to take into account the mechanical constraints such as the maximal load but also dimensional constraints to provide flexibility and independency to customers. The main constraints related to the mechanical design are described below.

The vehicle have been designed to transport a euro-pallet of 1.2m by 0.8m so it must to be able to carry a load of 1525kg evenly distributed. This payload corresponds to the weight of pallet and its maximum payload (Epal-pallets, 2016). The standard pallet is presented in Figure 2.

Figure 2. Epal-pallet.

In order to respect Akéo Plus strategy of customers' autonomy for modifications, the vehicle must be able to transport different types of loads as long as they respect the loading conditions defined by its first purpose. It must also have a mass lower than 500kg to be transported with a small truck.

The sales target of this AGV is 20 vehicles per year. So in order to avoid extra storage fees, the manufacturing processes have been considered for a manufacturing batch size of 20 vehicles per year.

To guarantee Akéo Plus competitiveness on the market of material handling, the vehicle must carry high-loads with low costs. To fulfil this last requirement, the cost reduction has been considered all along the designing process and used as an optimisation criteria for the selection of technical solutions.

The deliverables for the project were:

- A technical report
- A CAD model of the designed AGV
- A cost estimation of the mechanical structure of the vehicle
- A proof of good functioning

The proof of good functioning wasn't clearly defined. The idea was to convince the project manager and the company that the system works and fulfils requirements. It was the responsibility to the author to decide if prototypes and test rigs were required or if calculation model were good enough to be convincing.

1.3 Delimitations

This study was focused on the mechanical development of the AGV, so the technical solutions related to battery capacity and power control haven't been discussed in this study as well as the type of motors used to move the vehicle and their power. These components have been defined as input values for the study.

The embedded electronic systems and guidance systems were neglected in this study. Since they are small and light, it has been assumed that they can be incorporated to the vehicle in a second stage of its development without any modifications of the mechanical system.

The aesthetic aspect of the vehicle haven't been discussed in this study and the outer frame of the vehicle is out of the scope. In fact, the outer frame will be designed later to integrate all safety and vision systems in a good looking product. In fact, this study was focused on the mechanical resistance of wheels and chassis.

The manufacturing processes have been discussed in this study to take relevant decision for cost reduction, assembling and material selection. However the manufacturing plans, tolerances and detail drawings were out of the scope.

During the designing process other delimitations were set. These delimitations were not defined in the initial scope because they are related to problems that appeared during the study and couldn't be solved with means and time allocated. These delimitations are describe in the designing process to give a better understanding to the reader of the reasons for which they were added.

1.4 Method

The different steps of the methodology used to address the problem are described in this part.

Literature review and concept analysis

The first step performed in this study was a literature review. This review aimed to gather and analysis the existing knowledge on AGVs and mecanum wheels. This research also included an analysis of existing technologies and the most common problems encountered during the design of an AGV.

An analysis of the existing design of mecanum wheels was performed in parallel of the literature review to have a better understanding of the phenomena described in literature and to discuss the technical choices made for the first design.

The analysis of the existing prototype is included in the frame of reference chapter even if it has been performed during this study. This structure have been selected to have a direct comparison between the knowledge found in literature and the phenomena observed on the prototype.

Structural analysis

Based on the literature review and analysis, the system have been decomposed in mechanical units. A structural analysis of efforts applied on each mechanical unit was then performed. This analysis aimed to determine all efforts that have been used as input data for the detail design of mechanical units.

Since the system has a complex geometry which can hardly be simplified in plan problems, mechanical torsors have been used to determine efforts in this three dimensions problem. A quick reminder on mechanical torsors is provided in Appendix A.

In can be noticed that the structural analysis would have been performed with a software like MSc. Adams or Solidworks. However, performing the analysis by hand offered a better understanding of the system.

Detailed design

Using results from the structural analysis, every mechanical unit has been further designed. This part included a research of technical solutions and standard components selection. The new design was then drafted using Solidworks, a CAD software.

A study of mechanical resistance was realised on components obtained in CAD. Several methods were used to validate components resistance depending on efforts and geometry. The validation criteria used in this study is a safety factor defined by the equation(1).

$$Sf = \frac{\sigma_{yelding}}{\sigma_{c,\max}} \tag{1}$$

Where $\sigma_{yielding}$ is the yielding limit of the material and $\sigma_{c,max}$ is the maximum of Von Mises stresses in the considered component. A target value of 2 for the safety factor was set to design all components, since it's a good compromise between safety and product cost. However, since other parameters were taking into account during the designing process some components have higher safety factors.

The material selection for components was based on material properties and cost. Only standard materials which are already available in all subcontractors stock were selected. Using these materials avoid to have an extra cost on components due to material supply.

Components were optimized until the final design was reached. The optimisation process wasn't furthered to its full potential. In fact, the costs related to the study of these particular points would have been higher than savings that it would imply.

Test rigs and costs

In order to validate the design and complete the study, subcontractors and furnishers have been consulted to have production costs of the vehicle and a prototype of wheels has been manufactured. Test rigs had been designed and the prototype were then tested on several test rigs to validate wheels' performances.

2 FRAME OF REFERENCE

This chapter summarise the various concepts of mecanum wheels and existing knowledge on the subject. This chapter also includes common knowledge used during the designing process.

2.1 Working principle of mecanum wheel

A mecanum wheel is composed of a central hub, a series of rollers which are attached to the circumference of the hub and a motor which provides power to the wheel. The rollers are attached to the hub with rotating joints so they can freely rotate around their axes. As it can be observed in Figure 3, the rotation axes of rollers aren't parallel to the rotation axis of the wheel.

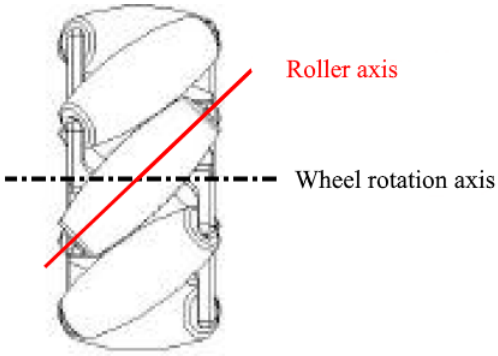

Figure 3. Traction force of mecanum wheel

Mecanum wheel can be designed with different angles between rollers' axes and wheel rotation axis depending on their utilisation. The wheel can even be designed with a variable angle to enhance their efficiency (Diegel et al., 2002). In this study, only the most common case, an angle of ±45°, was investigated.

The AGV is equipped with four mecanum wheels, two with an angle of 45° and two with an angle of -45°. The wheels can be assembled with two different configurations which are represented in Figure 4.

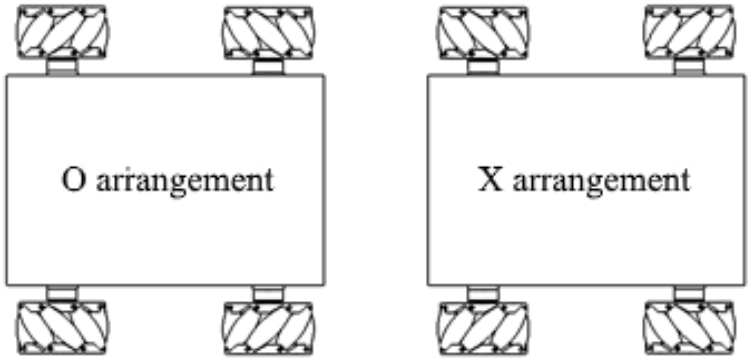

Figure 4. Mecanum wheels arrangements

From these configurations and with an appropriate control of wheels, the AGV is able to move in any direction.

Indeed, when a wheel is rotating, a traction force appears between its rollers and the floor. Due to the particular geometry of the wheel, the produced force is collinear to the rotation axes of rollers (De Villiers and Tlale, 2008), (Matsinos, 2012). The wanted traction force on the AGV is

then obtained by balancing forces acting on each wheel in order to get the right displacement (Taheri et al., 2015). Some possibilities of displacement with corresponding rotations of wheels are presented in Figure 5.

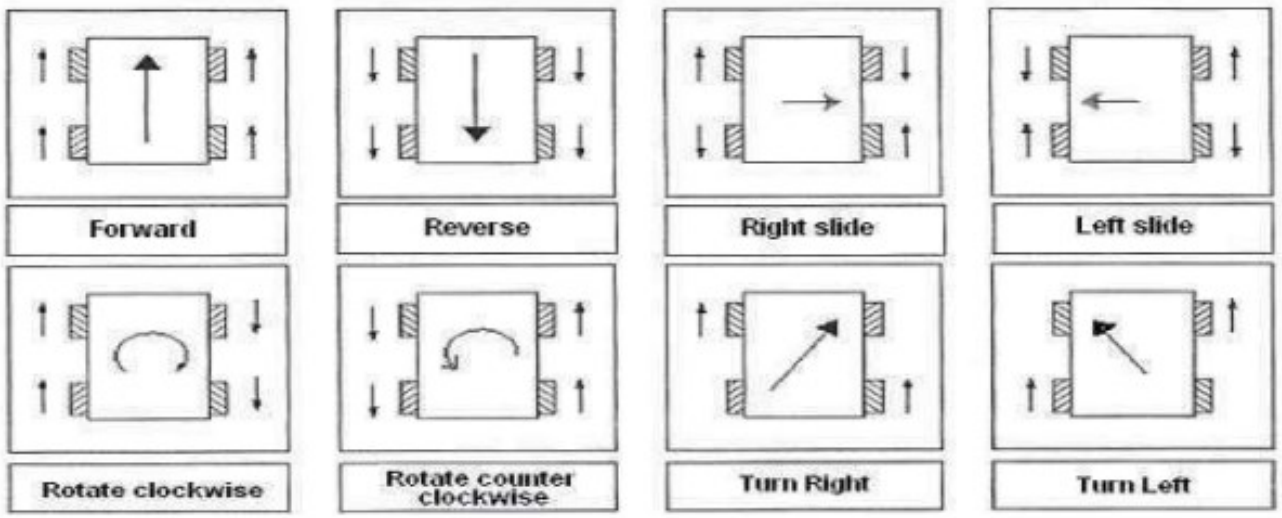

Figure 5. AGV displacements with four mecanum wheels in X arrangement.

2.2 Existing designs of mecanum wheel

Initial concepts of mecanum wheel

The mecanum wheel was invented by Bengt Erland Ilon (1972) with two different concepts. The first concept is composed of a central hub on which ground engaging parts are attached. The ground engaging parts are composed of a roller, its axis and an axis support attached to the central hub. This concept can be observed in Figure 6.

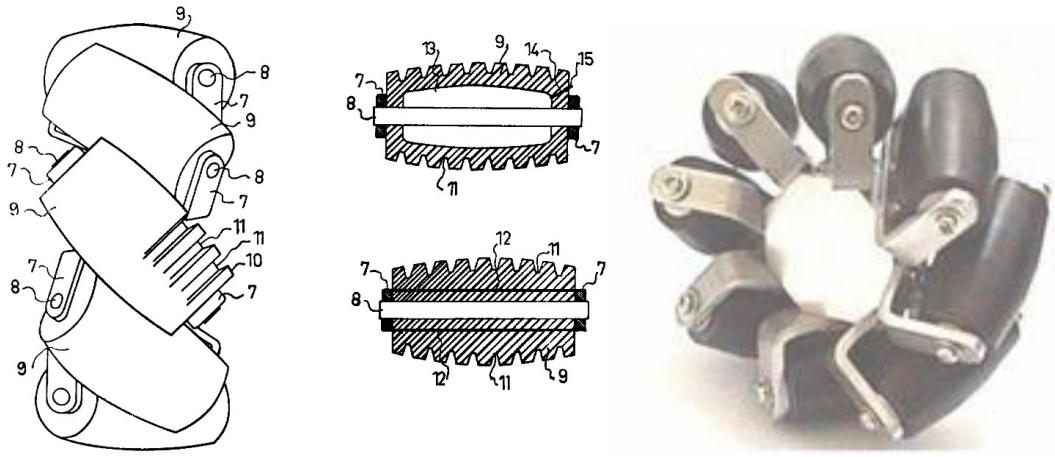

Figure 6. First concept of mecanum wheel from B.E. Ilon.

This concept is meant to be used with a large range of rollers and axis technologies and so used in a wide range of conditions and environments. This solution also guarantes an easy maintenance with its system of engaging parts that can be quickly disassembled and replaced.

For the second concept, roller axes, axis supports and hub are directly made of one component and rollers are split into two parts. This concept can be observed in Figure 7.

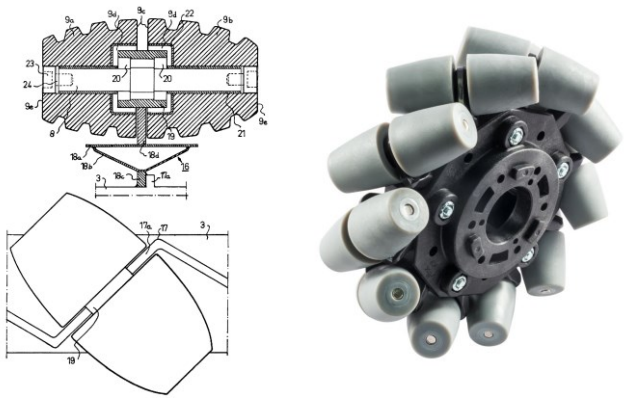

Figure 7. Second concept of mecanum wheel from B.E. Ilon.

This concept is still extensively used nowadays since it reduces the number of components and split rollers protect the hub against shocks during lateral movements of AGV.

Mecanum wheel for heavy loads

From these previous concepts, different types of mecanum wheels able to carry heavy loads have been invented.

The first concept is composed of a central hub on which roller axes are directly attached on both sides. Several rows of rollers are attached to the hub to increase the contact area and so reduce the contact pressure. In this concept, rollers' axes are unaligned to improve the circularity of the wheel and so improve piloting conditions (Potter, 2009). A picture extracted from the patent application can be find in Figure 8.

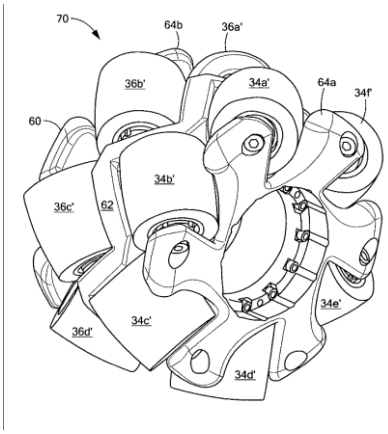

Figure 8. Concept of mecanum wheel for heavy loads from Potter.

However, as it can be observed on the figure, the hub has a very complex geometry and so its manufacturing is expensive.

The following solution is based on the second concept of Bengt E Ilon shown in Figure 7, the wheel is composed of a set of hubs, with split rollers, which are attached together. Since rollers' axes are aligned, with this solution a large number of hubs can easily be attached together. The wheel has then a large number of rollers in contact at the same time, so it reduces the contact pressure on each of them. This solution also offers an improved circularity and a low sensitivity of wheel to floor imperfections (Zdrahal et al., 2012). The concept is presented in Figure 9.

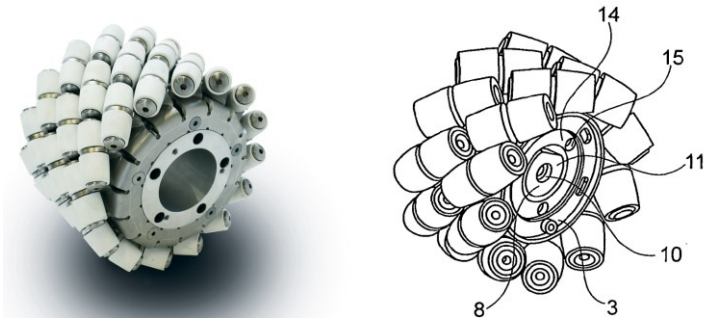

Figure 9. Concept of mecanum wheel for heavy loads.

The last solution is based on the first design of Bengt E Ilon but instead of attaching rollers' axes on independent supports, rollers' axes are attached to two rims. This solution reduces the number of components but it also increases the strength of the wheel. In fact, rims can be design to carry heavy loads. As it can be observed in Figure 10, this concept is more compact than the previous ones. However it doesn't improve the circularity of the wheel and it doesn't increase the contact area so it requires stronger materials for rollers.

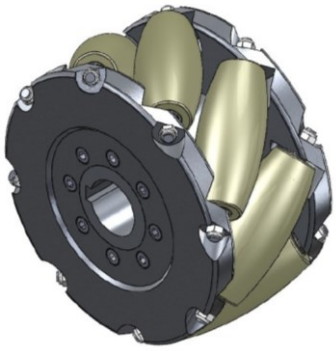

Figure 10. Selected concept of mecanum wheel for heavy loads.

From the three most common concepts of heavy load mecanum wheel which are presented above, the last one is the only one which isn't protected by an active patent, so this concept is the one that have been selected.

2.3 Common models used

Hertzian contact

A Hertzian contact occurs when there is a point or a line contact between two bodies. Due to the geometry of contact, a specific constraint distribution appears between the bodies when a force is applied. The most commonly used model to describe this phenomenon has been developed by Hertz (1881). The following parameters related to materials and geometry of bodies are introduced in Equations (2) and (3).

$$\frac{1}{R'} = \frac{1}{R_{1x}} + \frac{1}{R_{1y}} + \frac{1}{R_{2x}} + \frac{1}{R_{2y}} \tag{2}$$

$$\frac{1}{E'} = \frac{1-\nu_1^2}{2 \cdot E_1} + \frac{1-\nu_2^2}{2 \cdot E_2} \tag{3}$$

Where R_{1x} and R_{1y} are curvature radii in x and y directions of the body 1 and E_1 and ν_1 are respectively Young's modulus and Poisson's ratio for the same body. The notations with

subscript 2 correspond to the same parameters for the body 2. In order to simplify equations, the following notations are introduced.

$$\lambda = \frac{R_{1y} \cdot R_{2y} \cdot (R_{1x} + R_{2x})}{R_{1x} \cdot R_{2x} \cdot (R_{1y} + R_{2y})} \qquad \frac{1}{\kappa} = 1 + \left(\frac{\ln(16/\lambda)}{2 \cdot \lambda} \right)^{1/2} - \ln(4)^{1/2} + 0.16 \cdot \ln(\lambda) \tag{4}$$

The semi-axis A of the elliptic contact is then given by the Equation (5).

$$A = \kappa \left[1 + \frac{2\left(1-\kappa^2\right)}{\pi \cdot \kappa^2} - 0.25 \cdot \ln(\kappa) \right]^{1/3} \cdot \left(\frac{3F \cdot R'}{E'} \right)^{1/3} \tag{5}$$

And the semi-axis B is given by the Equation (6).

$$B = \left[1 + \frac{2\left(1-\kappa^2\right)}{\pi \cdot \kappa^2} - 0.25 \cdot \ln(\kappa) \right]^{1/3} \cdot \left(\frac{3F \cdot R'}{E'} \right)^{1/3} \tag{6}$$

Where F is the applied force.

The maximum contact pressure also called Hertzian pressure can then be deduced with the following equation.

$$P_0 = \frac{3F}{2\pi \cdot A \cdot B} \tag{7}$$

And the maximum shearing stress can be determined with the equation below.

$$\tau_{\max} = 0.310 \cdot P_0 \tag{8}$$

The maximum shearing stress is used as a dimensioning criteria for Hertzian contacts.

Bolted joints

Bolted joints are commonly used because they provide a cheap, simple and easy way to assemble two components without any relative motion. However they involve complex phenomena and they are still not perfectly modelled. The simplified model used in this study is presented in this part.

In order to keep contact between the components which are attached together, the screw is tightened in order to apply a pre-tensioning force on components. The pre-tensioning force, $F_{p,}$ which must be applied to guarantee a constant contact between components is given by the following equation.

$$F_p = F \frac{K_s}{K_s + K_c} \tag{9}$$

Where F is the force that the screw must handle and K_s and K_c are respectively the stiffness of the screw and the stiffness of components.

The stiffness of the screw is given by the equation below.

$$K_s = \frac{\pi}{4} \cdot \left(D - 0.9382 \cdot p \right)^2 \cdot \frac{E_s}{L} \tag{10}$$

Where D is the screw diameter, p is the pitch, E_s is the Young's modulus of the screw and L is the length of bolted joint.

The stiffness of components is obtained with the following equation (Junivall, Marshek, 2006).

$$K_c = \frac{\pi}{4} \cdot \left[\left(\frac{3 \cdot D + L \cdot \tan(30°)}{2} \right)^2 - D^2 \right] \cdot \frac{E_c}{L} \tag{11}$$

Where E_c is Young's modulus of components.

Other models can be used, especially to determine components stiffness with a better accuracy. This model has been selected because it provides a good approximation with simple parameters which are always known by the designer.

3 THE DESIGN PROCESS

The designing process is described in this chapter. This process begins with a structural analysis of the vehicle and wheels. Based on results of the analysis, each subsystem and component is further decomposed and analyzed to get the final design. The test rigs used to validate performances are also described in this chapter.

3.1 Initial design of AkeoPlus mecanum wheels

The initial design of mecanum wheel realised within the company was based on draughtsmen's experience and a first prototype had been manufactured to validate technical solutions. Since this design has been a starting point for this study, selected solutions are described in this part. The initial design is shown in Figure 11.

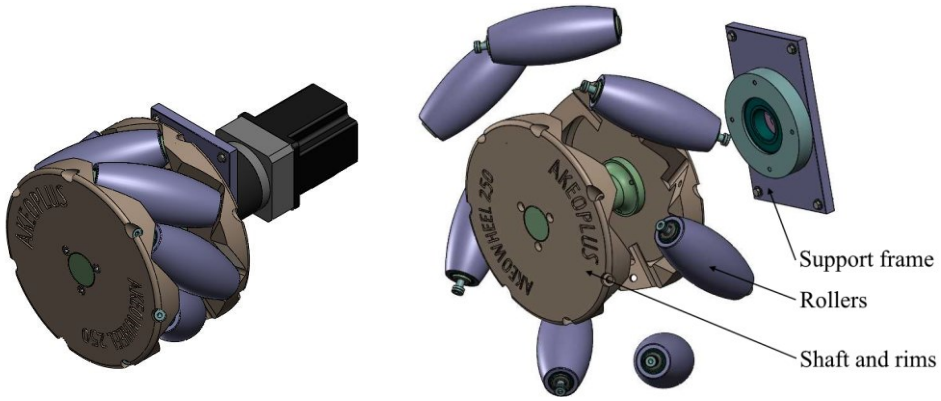

Figure 11. Initial design of mecanum wheel.

The design of this prototype can be decomposed in three mechanical units which are rollers, support frame and shaft and rims. These mechanical units are described one by one since each of them have its own technical solutions. Furthermore any change on these units has a low impact on the rest of the design and especially on calculation models.

Rollers

Each roller was mainly composed of an ellipsoid made of contact material which is rotating around an axis attached to the rims. Shaft and roller are presented in the figure below.

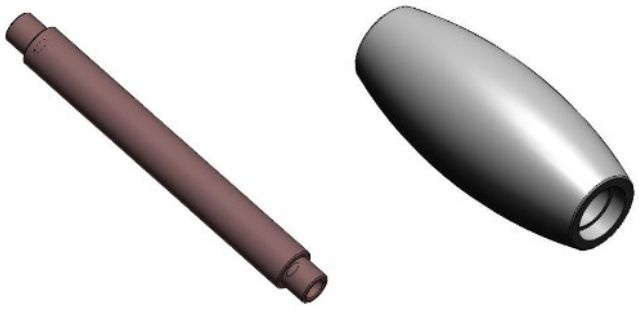

Figure 12. Initial designs of rollers and their axes.

The ellipsoid was made of PMMA, this material had been selected for its high hardness and its low price. The shape of ellipsoid had been approximated by a torus. According to Gfrerrer (2008), the error made by manufacturing a torus instead of an ellipsoid is lower than tolerances

with standard machining. So this approximation reduced manufacturing costs and complexity of the component. Since the ellipsoid shape of this first design follows recommendations found in literature, this point haven't been further discussed in this study.

The axis was made of aluminium and the guidance between axis and ellipsoid was realised by ball bearings as it can be observed in Figure 13.

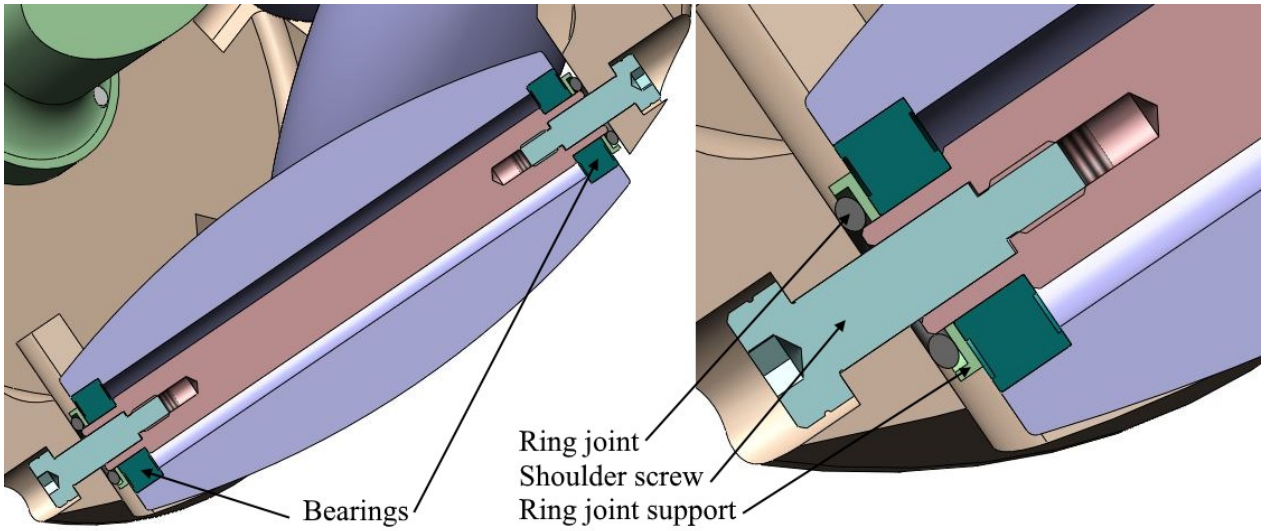

Figure 13. Initial design of rotating guidance of rollers.

The axis was attached to rims with shoulder screws. This type of screw was used to provide an accurate positioning of screwed components. This accuracy was required in this case to have a good radial positioning of rollers and so a good circularity of wheel.

Ring joints and their supports were placed between rims and ball bearings in order to keep ellipsoid in central position. This solution avoided accurate manufacturing which might imply extra costs and it also reduced impact noise when the ellipsoid moved from one side to the other.

Rims and shaft

Rims and shaft were designed in three different aluminium components, one shaft and two rims, to reduce manufacturing costs. In fact, the manufacturing process selected was machining and so the decomposition in three components reduced material needed as well as machining time. Since two types of mecanum wheels are required for one AGV, left and right ones, and both can use the same shaft, this decomposition lowered costs by component standardisation process. The assembly of the three components is presented in Figure 14. It can be observed that the components were screwed together to provide a simple and efficient assembling.

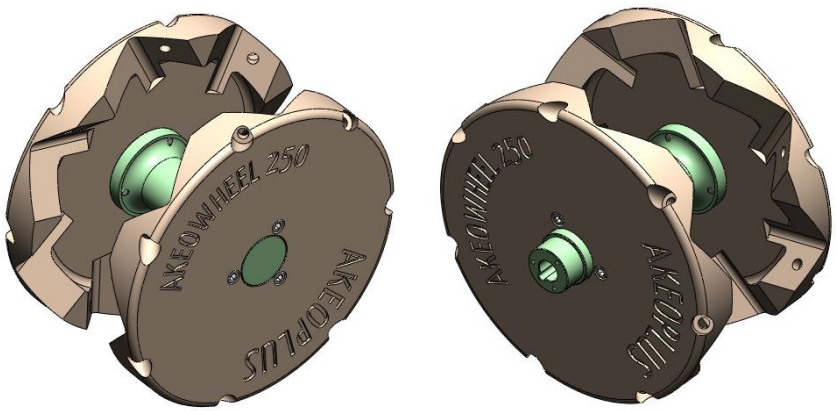

Figure 14. Initial design of rims and shaft assembly.

According to The Data Book from Cambridge University (2003) and considering estimated batch size of AGV, casting process could be used to make the assembly in one component. However this process produces components with high roughness and there isn't any foundry close to the company. So this solution had been set aside for aesthetic and logistic reasons. Based on the same strategic decisions, the casted solution haven't been investigated in this study.

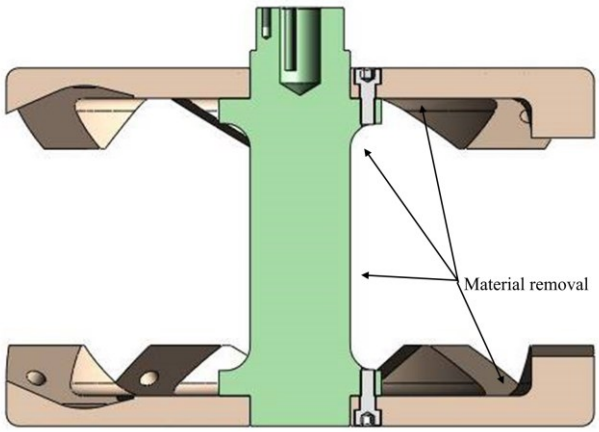

Figure 15. Material removal on initial design of rims and shaft assembly.

It can be observed in Figure 15 that some extra material removals were realised on shaft and rims to reduce total mass of wheel. In fact, even if mass isn't a key requirement of the product it still need to be considered to have a competitive product.

Support frame

The support frame was made of a bearing housing and a connecting plate. Both components were in aluminium. Housing was screwed to the plate to have a solution easy to assemble, simple and which could be connected to different types of connecting plate.

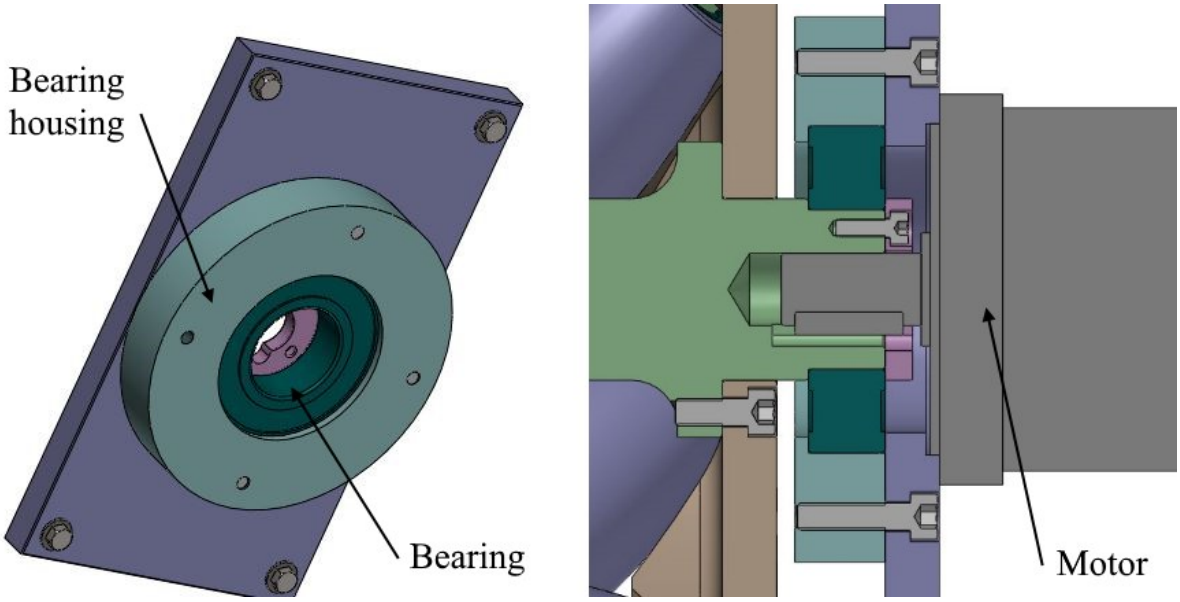

Figure 16. Initial design of support frame.

It can be observed on Figure 16 that the rotating guidance was realised by only one bearing on the CAD model. But since the motor has a ball bearing in output, the shaft was guided by two bearings in reality.

3.2 Prototype observations with the initial design

A first set of wheels had been manufactured with Akéo Plus initial design in order to validate technical solutions and have a better insight of problems related to the use of mecanum wheels. At the beginning of this study, tests were performed on wheels behavior to isolate unwanted phenomena. After observations, the system has been disassembled to check components' resistance and wear.

Vehicle vibrations

During prototype testing, it has been observed that the upper plate of the vehicle was moving randomly. These movements could be assimilated to vibrations with a low frequency. After some extra tests it appeared that these movements were induced by the non-circularity of the wheel. In fact, each corner of the plate was moving up and down during rollers transitions of the corresponding wheel. It can be found in the literature (Bae and Kang, 2016), that these vibrations are a common problem with mecanum wheels. These vibrations are induced by the fact that wheels aren't perfectly circular. The non-circularity is due to the wheels' geometry and the deformation of rollers implied by the contact pressure.

In other types of wheel the deformation only creates a difference between the theoretical diameter of the wheel and the actual one. But with a mecanum wheel when there is a transition between two rollers, the contact properties change due to variations of contact area and rollers' stiffness. These variations change the actual radius of the wheel and so it creates vertical vibrations. To improve the circularity of the wheel, two roller geometries have been investigated, one based on an experimental research realized by Guenther (2008) and another one based on a mathematical model. The second geometry has been obtained by determining the circle which fits the best the ellipsoid and without considering any deformation effect of rollers since they are made with a hard material.

Unusual wear of the motor

After vibration tests, the wheels have been disassembled to get more informations on components and their wear. It appeared that the motor shaft had abnormal wear as it can be observed on Figure 17.

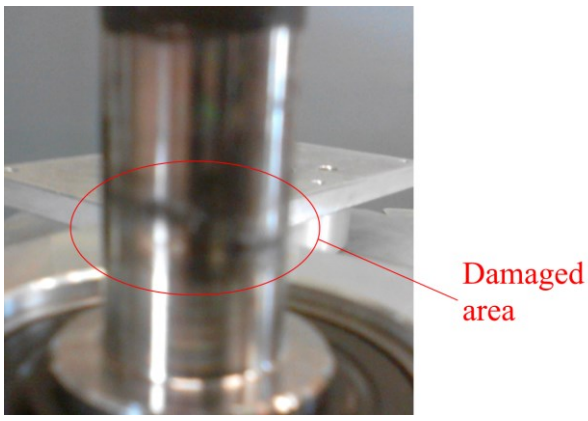

Figure 17. Wear of motor shaft.

It has been deduced that this wear was due to a lack of stiffness of the bearing arrangement. In fact, bearings were attached to different components and the key coupling wasn't stiff enough to guarantee good guiding conditions. A solution with the two bearings attached on the shaft has been developed in this study to solve the problem.

3.3 Structural analysis of AGV

In order to know the forces applied on each component, a structural analysis has been performed on the AGV and on the mecanum wheels.

Calculation model of the vehicle

The structural analysis of the AGV has been performed on a simplified model of the vehicle composed of four mecanum wheels and a chassis. This simplified model has been selected to enable a quick dimensioning of the vehicle with a low dependency on characteristics of wheels and support frame.

The AGV has been designed to transport heavy loads so it's carefully loaded by other machines or by operators assisted by machines. It can then be assumed that the load is equally distributed on wheels. Since the vehicle carries heavy loads, it will also moves slowly within the workshop for safety reasons. It has also been assumed that the inertial forces are insignificants compare to others forces. The model used in static position is presented in Figure 18.

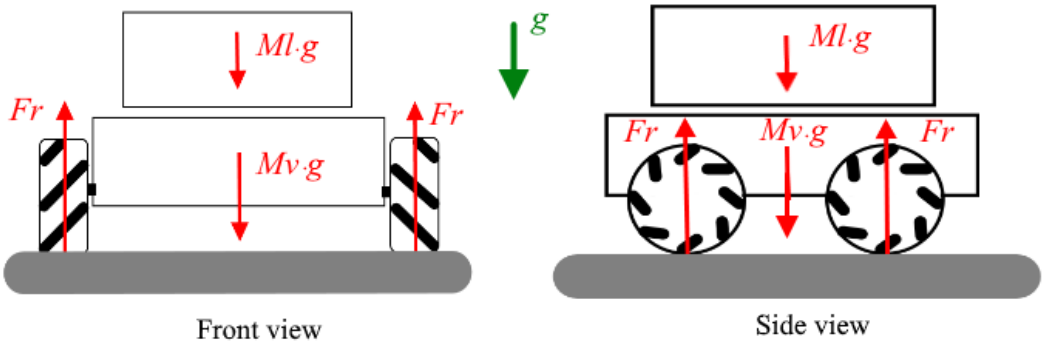

Figure 18. Static equilibrium of the AGV.

Using notations from the figure above, the reaction force of the floor is given by the following equation.

$$Fr = \frac{(Ml + Mv) \cdot \mathrm{g}}{4} \tag{12}$$

When the vehicle is moving, adhesion forces appears between floor and wheels. These forces are named *Ff* and presented in Figure 19 considering the wheels' geometry and two moving cases.

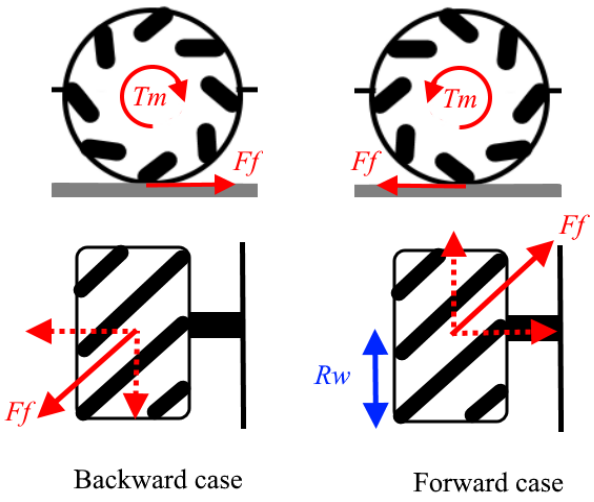

Figure 19. Traction force of wheels.

It has also been assumed that wheels don't slip on the floor and there is no power loses in the system. The adhesion force is then related to the maximum motor torque, *Tm*, by the equation (13) in both cases.

$$Ff = \sqrt{2} \cdot \frac{Tm}{Rw} \tag{13}$$

Numerical results

The radius of wheels as well as the maximum motor torque have been selected considering some parameters such as energy consumption and maximum speed of AGV. Since this part of the designing process was out of the scope of this thesis, numerical values of these notations have been used as input data. At this point of the study, the actual mass of the vehicle was unknown, so the maximum vehicle mass defined in requirement specifications has been used as input value. Input values used for the structural analysis of vehicle are presented in Table1.

Table 1. Input values for structural analysis of AGV

Maximum mass of transported loads	*Ml*	1525 kg
Mass of the vehicle	*Mv*	500 kg
Gravity constant	*g*	9.81 m/s²
Maximum torque provided by the motor and the reducer	*Tm*	75.6 Nm
Wheel radius	*Rw*	125 mm

From the previously obtained equations and input values in Table 1, the following results have been obtained.

Table 2. Results for structural analysis of AGV

Reaction force of the floor	*Fr*	4966 N
Adhesion force between a wheel and the floor	*Ff*	855 N

Since the reaction force and the adhesion force on a wheel have high values, it has been assumed for the structural analysis of the wheel that weight can be neglected compare to other forces.

3.4 Structural analysis of the wheel

The wheel has been further decomposed in subsystems following observations and decomposition in mechanical units made in description of Akéo Plus initial design. This decomposition can be observed in Figure 20 as well as numbers allocated to each sub system.

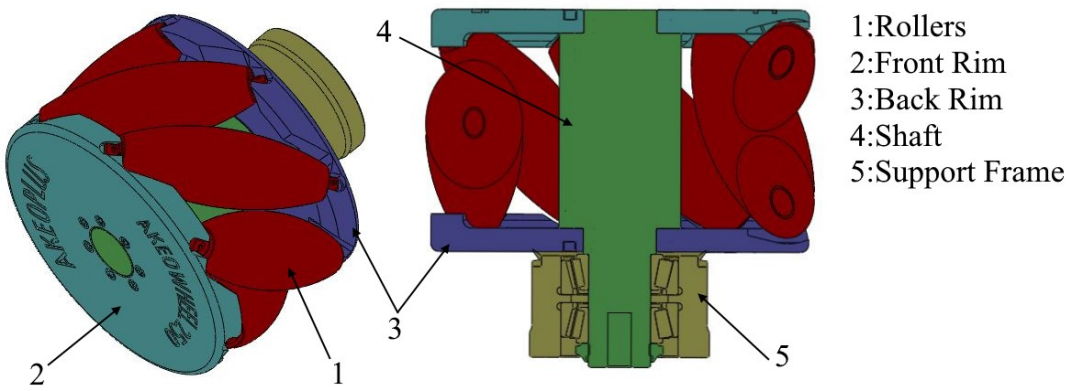

Figure 20. Decomposition of wheel in subsystems.

Static equilibrium of rollers

When the wheel is rotating, the contact point moves along rollers and goes from one roller to another through a transition area. In this transition area, there is two rollers in contact with the floor at the same time. It has been assumed that mechanical efforts on a roller are lower during a transition. Considering this assumption, only the relevant area of rollers has been studied during the structural analysis. The studied area and its related angle are presented in Figure 21.

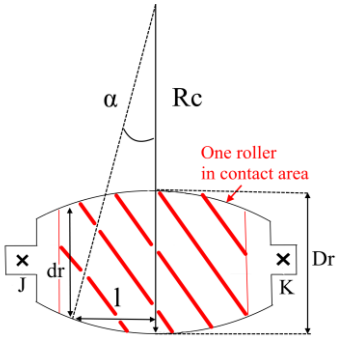

Figure 21. Studied area of rollers.

The angle α has been used as a variable to define the position of the contact point for the rest of the structural analysis.

Rollers are in contact with the floor and attached to the front and back rims. The mechanical torsors of these attachment have been developed with the following forms:

$$\{\tau(2\to1)\}=\begin{Bmatrix} X_{21} & 0 \\ Y_{21} & 0 \\ 0 & 0 \end{Bmatrix}_{(J,x2,y2,z2)} \qquad \{\tau(3\to1)\}=\begin{Bmatrix} X_{31} & 0 \\ Y_{31} & 0 \\ 0 & 0 \end{Bmatrix}_{(K,x2,y2,z2)} \tag{14}$$

The static equilibrium of rollers is given by the equation (15).

$$\{\tau(2\to1)\}+\{\tau(3\to1)\}+\{\tau(\text{floor}\to1)\}=\{0\} \tag{15}$$

The forces on a roller with associated geometry are shown in Figure 22.

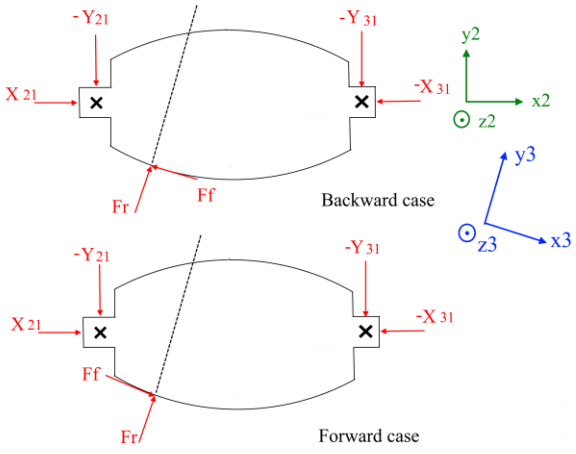

Figure 22. Forces applied on rollers.

It can be noticed that equations for the backward case can be derived from equations from the forward case by replacing Ff by –Ff. So equations for the structural analysis have only been

derived in the forward case but both case have been calculated. These equations can be found in Appendix B.

Since X_{21} and $-X_{31}$ are representing contact forces between the roller and rims, they can't be negative. This particularity has been taking in account during equation solving. The following values are used for numerical application.

Table 3. Input values for static equilibrium of rollers

Maximum diameter of rollers	*Dr*	62 mm
Curvature radius of rollers	*Rc*	242.4 mm
Distance between two attachment point of rollers	*L*	182 mm

The curves of forces depending on α obtained are presented in Figure 23.

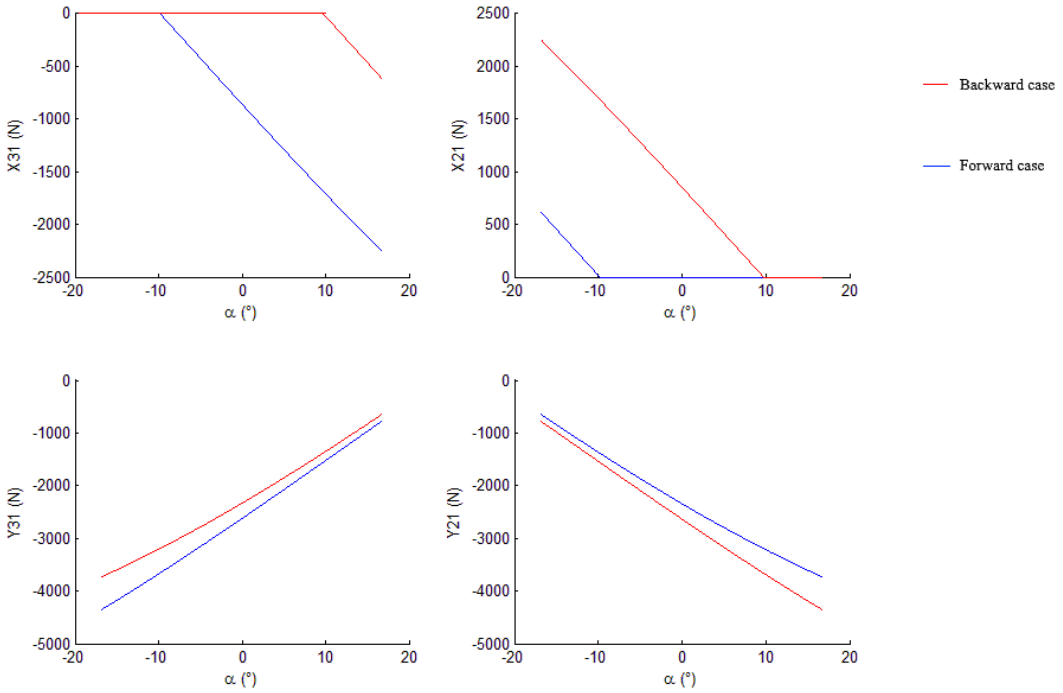

Figure 23. Curves of forces applied on rollers depending of α.

Static equilibrium of rims

Both rims are in contact with rollers and the shaft. Considering the hypothesis that only one roller at the time is loaded, it has been assumed that only one of them is in contact with rims. The geometry of rims and efforts applied on them are presented in Figure 24.

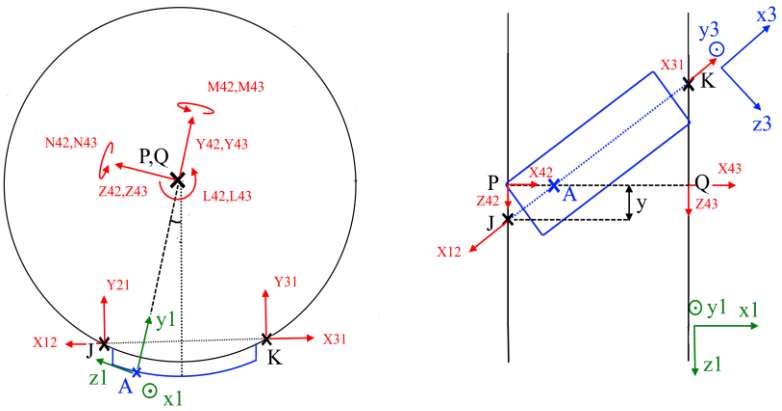

Figure 24. Efforts applied on rims.

In order to keep a simple model for this analysis, it has been assumed that attachment points on rollers and attachment points on shaft are in the same plane. Rims can then be modelled by flat disks.

The mechanical torsors of the contacts between the shaft and rims have been developed with the following forms:

$$\{\tau(4\to 2)\}=\begin{Bmatrix} X_{42} & L_{42} \\ Y_{42} & M_{42} \\ Z_{42} & N_{42} \end{Bmatrix}_{(P,x1,y1,z1)} \qquad \{\tau(4\to 3)\}=\begin{Bmatrix} X_{43} & L_{43} \\ Y_{43} & M_{43} \\ Z_{43} & N_{43} \end{Bmatrix}_{(Q,x1,y1,z1)} \tag{16}$$

So the static equilibrium of the front rim is given by the equation (17) and the one of the back rim is provided by equation (18).

$$\{\tau(1\to 2)\}+\{\tau(4\to 2)\}=\{0\} \tag{17}$$

$$\{\tau(1\to 3)\}+\{\tau(4\to 3)\}=\{0\} \tag{18}$$

Equations above have been solved using the properties of mechanical torsors presented in Appendix A. The curves of efforts depending on α obtained for the front rim are presented in Figure 25.

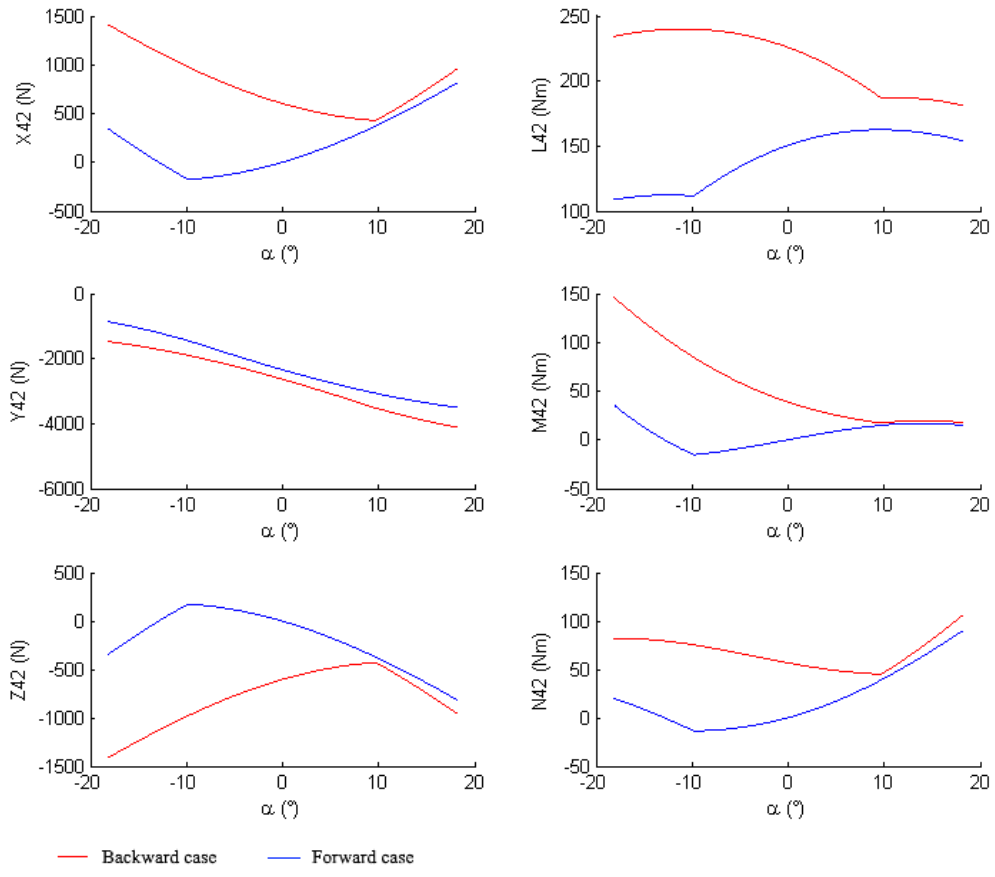

Figure 25. Curves of effort applied on the front rim depending of α.

These curves have been combined and compared to each other to check equations and point out model defaults which might appear. During this process it has appeared that the model used to determine L42 doesn't describe the actual geometry and so an error of around 1% was made during calculation. Since this error is low and its correction would terribly increase the complexity of the model, this error has been neglected for the rest of the study.

The curves of efforts obtained for the back rim are presented in figure 26.

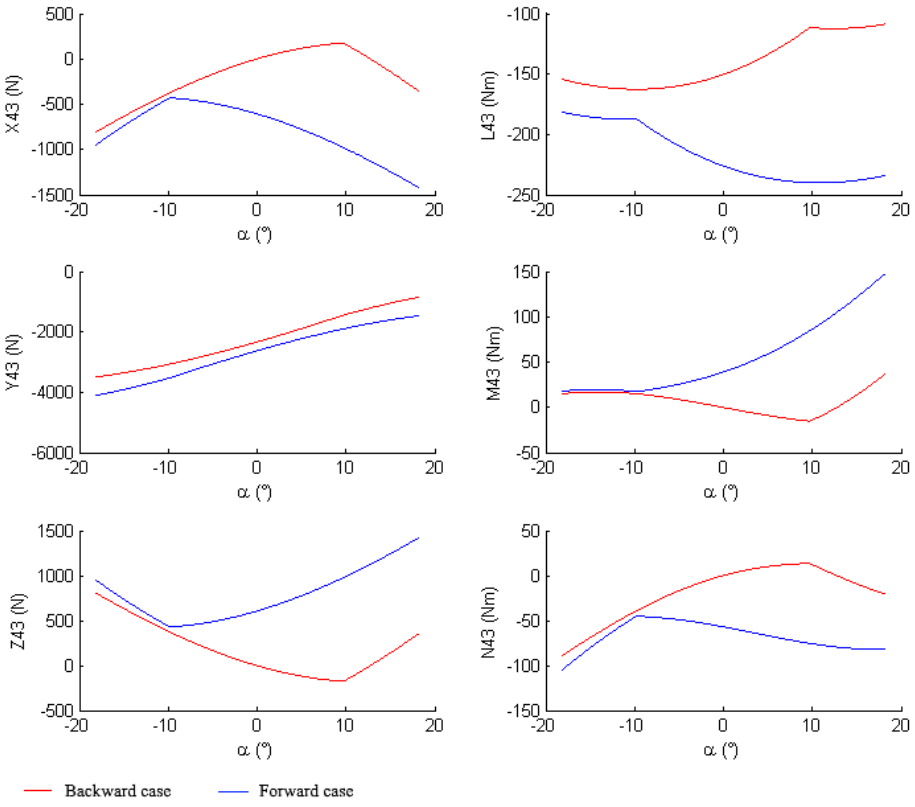

Figure 26. Curves of effort applied on the back rim depending of α.

Static equilibrium of shaft

The shaft is in contact with both rims, with the support frame through a set of two bearings and with the motor. In order to be able to use results from this structural analysis for bearing selection and dimensioning, the mechanical torsor of efforts between the shaft and the support frame has been decomposed in two distinct torsors, one for each bearing. The forces applied on the shaft and associated geometry are presented in Figure 27.

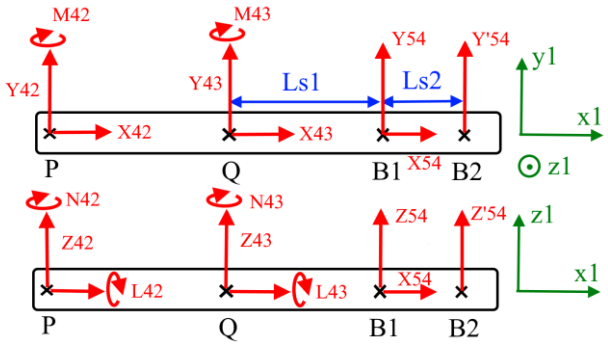

Figure 27. Efforts applied on shaft.

The mechanical torsors of the contacts between the shaft and the support frame have been developed with the following forms:

$$\{\tau(5\to 4)\}=\begin{Bmatrix} X_{54} & 0 \\ Y_{54} & 0 \\ Z_{54} & 0 \end{Bmatrix}_{(B1,x1,y1,z1)} \qquad \{\tau'(5\to 4)\}=\begin{Bmatrix} 0 & 0 \\ Y'_{54} & 0 \\ Z'_{54} & 0 \end{Bmatrix}_{(B2,x1,y1,z1)} \tag{19}$$

The common assumption that bearings can be modelled by spherical joints has been made so bearings aren't able to transmit a torque to the support frame in any direction.

The force in x1 direction which appears due to wheel geometry is transmitted to the support frame through one of the bearings. The determination of which bearing transmits this force depends of bearing arrangement so it couldn't be determined at this point of the study. Since the position of this force isn't influencing results for the structural analysis, it has been set that the force is in B1.

It has been assumed that the motor and the shaft are perfectly aligned so the torsor has the following form.

$$\{\tau(\text{mot} \to 4)\} = \begin{Bmatrix} 0 & Tm \\ 0 & 0 \\ 0 & 0 \end{Bmatrix}_{(P,x1,y1,z1)} \tag{20}$$

The static equilibrium of the shaft is given by the equation(21).

$$\{\tau(3 \to 4)\} + \{\tau(2 \to 4)\} + \{\tau(5 \to 4)\} + \{\tau'(5 \to 4)\} + \{\tau(\text{mot} \to 4)\} = \{0\} \tag{21}$$

The equations obtained after solving are presented in Appendix B and the numerical values of parameters are given in Table 4.

Table 4. Input values for static equilibrium of shaft

Distance between the back rim and the first bearing	*Ls1*	32 mm
Distance between the two bearings	*Ls2*	31 mm

The curves of forces depending on α are presented in Figure 28.

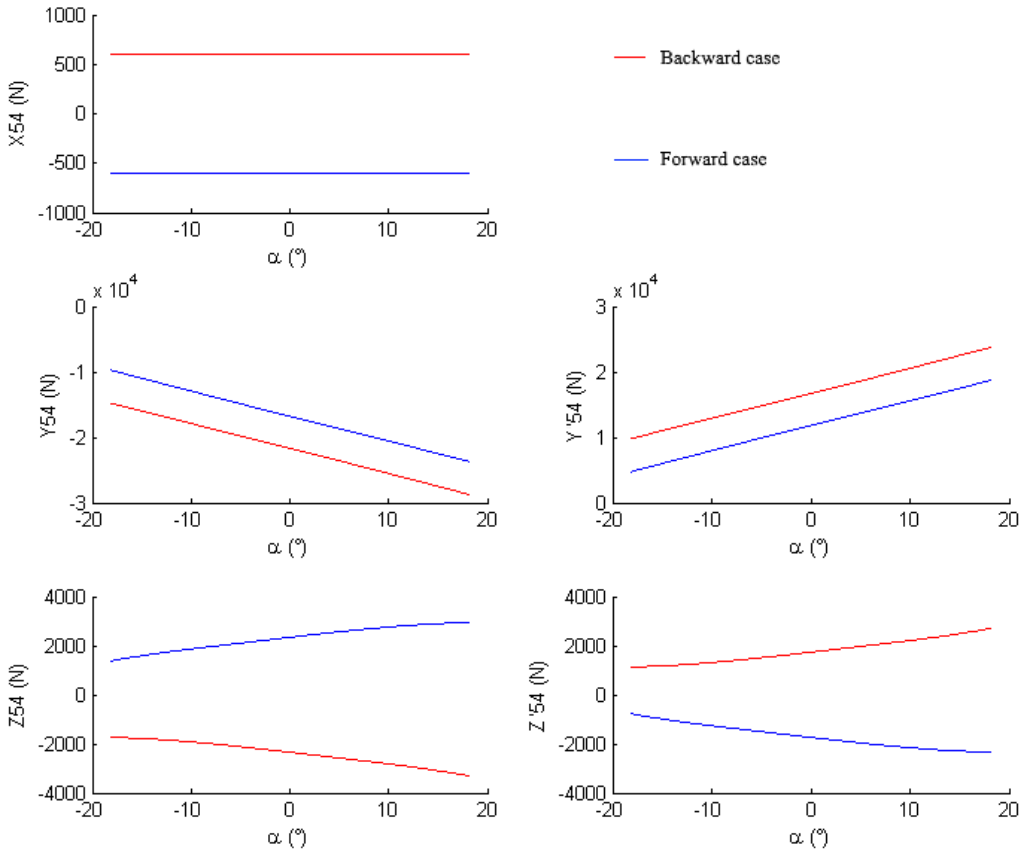

Figure 28. Curves of efforts applied on the shaft depending of α.

3.5 Subsystem 1: Rollers

The study of rollers includes a first part on rollers geometry in order to get rollers with a shape that reduces vibrations. The study of geometry is followed by a study of mechanical resistance of rollers and rollers' axes.

Rollers geometry

As it has been described in previous parts, ellipsoid shape of rollers can be approximated with a torus in order to reduce manufacturing costs. The radius which fits the best the ellipsoid, will be determined in this part as well as the difference between the torus and the ellipsoid.

To get a circle with a radius *Rw* when the ellipsoid is rotated by 45°, the ellipsoid presented in Figure 29 need to be considered.

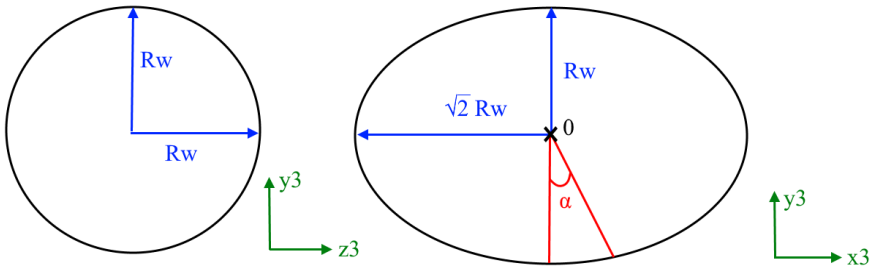

Figure 29. Ellipsoid shape.

Only the area defined by the angle α will be studied to determine the best radius since the rest of the ellipsoid is never in contact with the floor. The curvature radius is then given by the equation below.

$$\rho = 2 \cdot Rw \cdot \left(1 - \frac{1}{2} \cdot \left(\cos\left(\alpha + \frac{\pi}{2} \right) \right)^2 \right)^{3/2} \tag{22}$$

And the curvature centre is given by the following equations.

$$y = Rw \cdot \left(\cos(\alpha) \right)^3 \qquad x = \frac{Rw}{\sqrt{2}} \cdot \left(\sin(\alpha) \right)^3 \tag{23}$$

From the positions of the curvature centre, an average centre is calculated. Radii are calculated from the new curvature centre and the actual position of the point on the ellipsoid. The torus radius is then obtained by calculating the mean radius. A value of 242.4mm for the curvature radius is obtained. The difference between the torus and the ellipsoid can be observed in Figure 30.

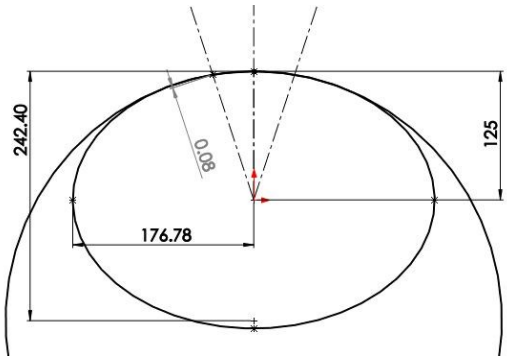

Figure 30. Torus deviation.

A deviation of 0.08mm is observed between the ellipsoid and the torus. Since the tolerance for standard machining is larger than the deviation, this result is in accord with Gfrerrer's study (2008).

According to Guenther, Wheels carrying high loads can have good rolling characteristics with a ratio of 1.10. The ratio introduced by Guenther is given by the equation below.

$$ratio = \frac{2 \cdot Rw}{Rc} \tag{24}$$

A curvature radius of 227.3 has been obtained with this method. Rollers with both curvature radius have been manufactured for comparison.

Contact between rollers and the floor

In order to validate rollers' dimensioning, the contact between the floor and rollers has been further studied. Using assumption from structural analysis about transition area of rollers, two critical points have been analysed. The first one is the point where α=0 because in this point the conformity of surfaces induce highest contact stresses. The second point is the one where α is at its maximum, just before the transition area. In fact, in this point side effects appeared due to the geometry of rollers. It has been assumed that other points imply lower stresses in material than these two points.

It has been assumed that the floor is made of concrete. The rollers are made of Polyurethane 95A instead of PMMA. This material has been selected because it provides low rolling resistance, good wear resistance and a higher load capacity than PMMA (Kauzlarich and Thacker, 1985). According to Qi and Boyce (2004), Polyurethane 95A has a complex behaviour which includes time dependence, softening and hysteresis. Since such complex behaviour would require a lot of time and expertise to be implemented in the contact study, the Polyurethane 95A is modelled by a linear elastic material with a Young's modulus of 120MPa (Basf, 2014) and a Poisson's ratio of 0.48 (Qi and Boyce, 2004). This simplification has reduced the accuracy of the contact study, however this particular point of the study can be developed later on if it's required. In fact, rollers are wear parts and they will probably be changed several times during wheel lifetime. So they can be replaced by improved versions without modifying the wheel architecture.

For the critical point where α is maximal, the contact doesn't meet hypotheses of Hertzian contact. So to estimate stresses in roller, a FEA has been conducted. The result is presented in Figure 31.

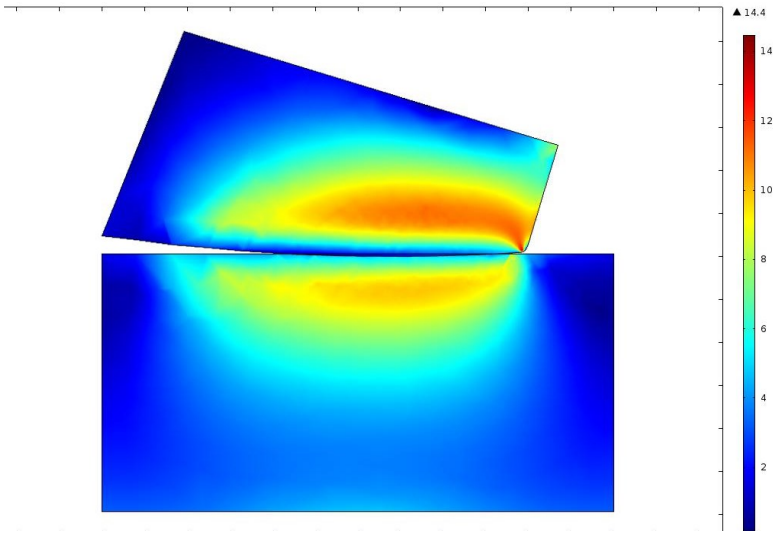

Figure 31. Contact stresses when α is maximal.

It can be observed that a maximum Von Mises constraint of 14.4 MPa has been obtained and as expected side effects appeared in this position. In this case the Hertzian pressure is equal to 22MPa.

For α=0, the contact meet hypotheses of Hertzian contact formulated by Ingelbert, Da Silva Botelho and Lemaire Caron (2011). The materials parameters used are presented in Table 5.

Table 5. Input values for Hertzian contact

Young's modulus of concrete	*Ec*	30 GPa
Poisson's ratio of concrete	*vc*	0.2
Young's modulus of Polyurethane 95A	*Ep*	120 MPa
Poisson's ratio of Polyurethane 95A	*vp*	0.48

At this point, the curvature radii of rollers are Rc and Dr/2. The applied force is Fr found during the structural analysis and it has been assumed that the floor is a flat surface. Using equations provided in the frame of reference, a maximum shearing stress of 6.3MPa and a Hertzian pressure of 20MPa are obtained.

The yielding limit of polyurethane is equal to 47MPa, so in both cases the rollers will handle efforts. However the main concern for the rollers in this study is the resistance of rollers' surface. In fact, if rollers are permanently deformed due to the contact pressure the wheel would quickly have a very bad circularity.

The first case is the one with the highest Hertzian Pressure, however results above have been obtained by considering there is pure rolling between rollers and the floor. If the extreme case of pure sliding is now considered, according to Hamilton and Goodman (1966), additional shearing stress with a maximum given by equation (25) appears at the surface of rollers.

$$\sigma_{r,max} = 2 \cdot \mu f \cdot P_0 \tag{25}$$

Where P_0 is the Hertzian contact pressure and μf the friction coefficient. According to Sunray researches (2015), the friction coefficient between polyurethane 95A and concrete is equal to 0.5.

In the critical case where α is at its maximum shearing stresses of 22MPa appears at the surface of rollers. Since no data have been found in literature on Polyurethane 95A surface pressure resistance in the studied case, a prototype and a series of tests are needed to compare the obtained results with reality and check the resistance of rollers.

Rollers' axes dimensioning

Rollers axes do the connection between rollers and rims. The shape presented in Figure 32 has been selected. In this new shape, rollers' axes have one hole and two flat spots at their two tips. This geometry enables a quick and easy maintenance of rollers. Even if the quick maintenance hasn't been defined as a requirement, it became necessary since rollers have been designed to be wear components in the FEA performed above.

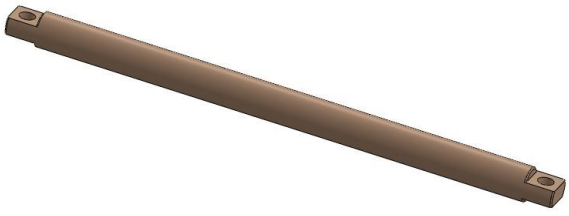

Figure 32. Geometry of rollers' axes.

As it can be observed in Figure 33, rollers axes are screwed on the outer surface of rims and so they have an easy access. With this fastening system, the roller can even be changed while the AGV is loaded in case of serious damages on a roller.

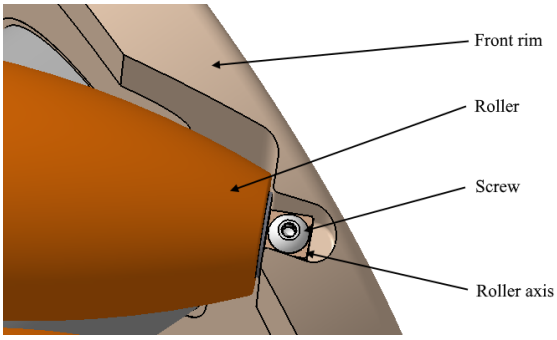

Figure 33. Attachment of rollers.

Rollers' axes are made of hardened steel which is rectified. This material has been selected because it has very good mechanical properties and it can be bought with standard diameter for a very low price.

It has been assumed that rollers axes are perfectly fixed relative to rims. The efforts applied by rollers on their axes are then creating pure shearing. The maximum shearing stress in rollers axes is given by the equation(26).

$$\tau_{rs,\max} = \frac{\max(Y_{12}, Y_{13})}{S_{rs}} \tag{26}$$

Where S_{rs} is the area of the sheared section and Y_{12} and Y_{13} are the radial efforts of rollers determined during the structural analysis. With an area of 62mm^2 for the sheared section and a maximum force of 4 355N, a maximum shear stress of 70MPa has been obtained. The hardened steel has a shearing resistance of 370MPa, so rollers' axes have been dimensioned with a safety factor of 5. This safety factor is higher than the targeted value but a reduction of axes' diameter would have a negative effect on guiding elements.

Guiding elements

The guiding elements between rollers and their axes are subjected to high efforts and low speeds. In fact the vehicle is moving slowly for safety reasons and so rollers rotate slowly around their axis. Due to these conditions, bushings are more appropriate than bearings and they are also cheaper. Wheels will be used in industrial environment with dust and dirt, so if a lubricant is used, it would often need to be cleaned or changed. Since it isn't reasonable to plan maintenance on bushings due to the quantity of bushings per vehicle, self-lubricated bushing have been selected.

It's reminded that rollers will be pushed against rims during wheel rotation, so in order to keep good sliding condition, flanged bushing are used. Rims are made of aluminium and rollers are rotating with many start and stop cycles. Due to these particular conditions, plastic bushing have been selected to avoid quick abrasion implied by Galling phenomena. Moreover bushing are attached to rollers and they are also wear parts, so they can then be changed frequently whereas rims shouldn't be replaced because of wear during product lifetime.

The mean pressure on bushing in radial direction is given by the equation(27).

$$P_{m,r} = \frac{\max(Y_{13}, Y_{12})}{D_{axes} \cdot L_b} \tag{27}$$

Where D_{axes} is the diameter of rollers axes and L_b is the length of bushings.

The mean pressure on bushing in axial direction is obtained by using equation(28).

$$P_{m,a} = \frac{4 \cdot \max(X_{13}, X_{12})}{\pi \cdot (D_{axes}^{\ 2} - D_b^{\ 2})} \tag{28}$$

Where D_b is the outer diameter of bushing flange.

The values used for numerical application are listed in Table 6.

Table 6. Input values for bushing selection

Diameter of rollers' axes	D_{axes}	14 mm
Maximum radial force on bushings	$\max(Y_{13}, Y_{12})$	4 355 N
Length of bushings	Lb	20 mm
Outer diameter of bushing flanges	Db	20 mm
Maximum axial force on bushings	$\max(X_{13}, X_{12})$	2 255 N

With these values, a radial mean pressure of 15.6MPa and an axial mean pressure of 14.0MPa have been obtained. A bushing with a maximum mean pressure of 60MPa and a good wear resistance has been selected to provide a safety factor of 3.5 and a long life time.

Screw selection

To select screws to fasten the rollers' axes on the rims, two types were studied: button head screw and socket head screw. The two types of screw are presented in figure 34. Button head screws have thinner heads and so they maximise the distance between the floor and the screws. Socket head screws are usually used because they have a good fatigue resistance and they can handle high tightening torques. In this case, there is low efforts on screws so the tightening torque will stay low compare to the maximum torque that button head screws can handle. So screws with button head have been selected instead of socket head screws.

Figure 34. Types of screw used.

To calculate the pretensioning force on button head screws, it has been assumed that the wheel is made in such way that the two screws of one roller axis are carrying the axial force applied on rims by the loaded roller. In reality, this force is distributed between all rollers axes and the bolted joints between the shaft and rims. However, this model has been used to provide an extra safety and to guaranty that the wheel won't fall a part in the case of shaft rupture.

This force are named X13 and X12 in the structural analysis and there maximum value is 2 255N. The model used is represented in Figure 35.

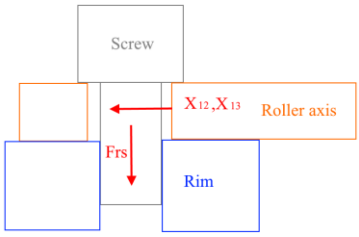

Figure 35. Screws pre-tensioning model.

In order to prevent sliding between rim and roller axis and so to keep good tightening conditions of screw, the tightening force must be higher than the one given by the equation(29).

$$Frs = \frac{\max(|X_{12}|,|X_{13}|)}{\mu_{al,s}} \tag{29}$$

Where $\mu_{al,s}$ is the friction coefficient between steel and aluminium. This coefficient has been considered to be equal to 0.5. The tightening force must then be higher than 4 510N. By using the model described in the frame of reference, a pre-tensioning force of 1 000N is necessary. According to VDI norm 2230, a M5 screw with a class 8.8 can provide a pre-tensioning force of 5 000N. So this type of screw responds to needs.

3.6 Subsystems 2 & 3: Rims

Rims make connection between rollers and the shaft. They are key components during the cost reducing process since they need to integrate the particular geometry of mecanum wheel for a low cost. In fact, the previous design of rims implied seven positioning on machining fixture during the manufacturing process and represented half of machining costs of wheels.

Changes on the rims design are presented in Figure 36. These changes are mainly related to the quick maintenance feature. Particularly because the flat spots on rollers' axes require matching surfaces on rims. Fillet edges have been added in corners to reduce stress concentrations and so increase the resistance of rims. Two other fillet edges have been drawn in the contact surface between rims and bushing to avoid quick wear of bushing that sharp edges could produce.

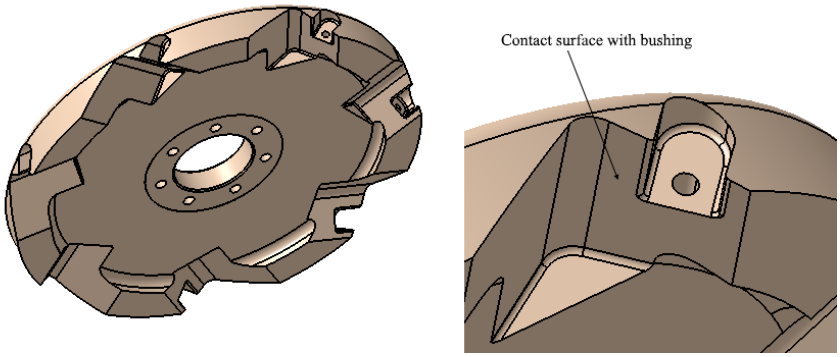

Figure 36. Geometry of rims.

It can also be observed in the previous figure that seven screws, one per roller, have been used to join rims with the shaft. This solution suppresses alignment mistakes during assembling and it also provides good symetry properties to rims and shaft.

The attachement and material removal for rollers have been designed in a such way that they can be made with one machining direction per roller as it can be observed in Figure 37.

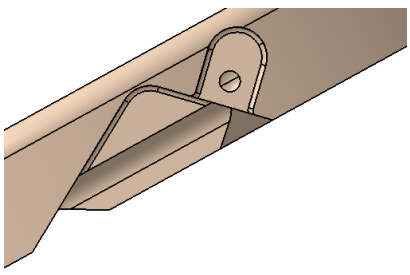

Figure 37. Manufacturing plan of roller.

With the modifications describe above, the rims can be machined on a 4-axes turning machine with only two positioning on fixture. This last point not only reduces rims' price but it also increases accuracy of machining.

Due to the complexity of geometry, a FEA has been performed to check mechanical resistance of rims and also to reduce their size and the amount of material used to manufacture them. Based on structural analysis a maximum force of 4 355N is applied on interface between rollers and rims. The Von Mises stresses and deformations related to this load case are presented in Figure 38.

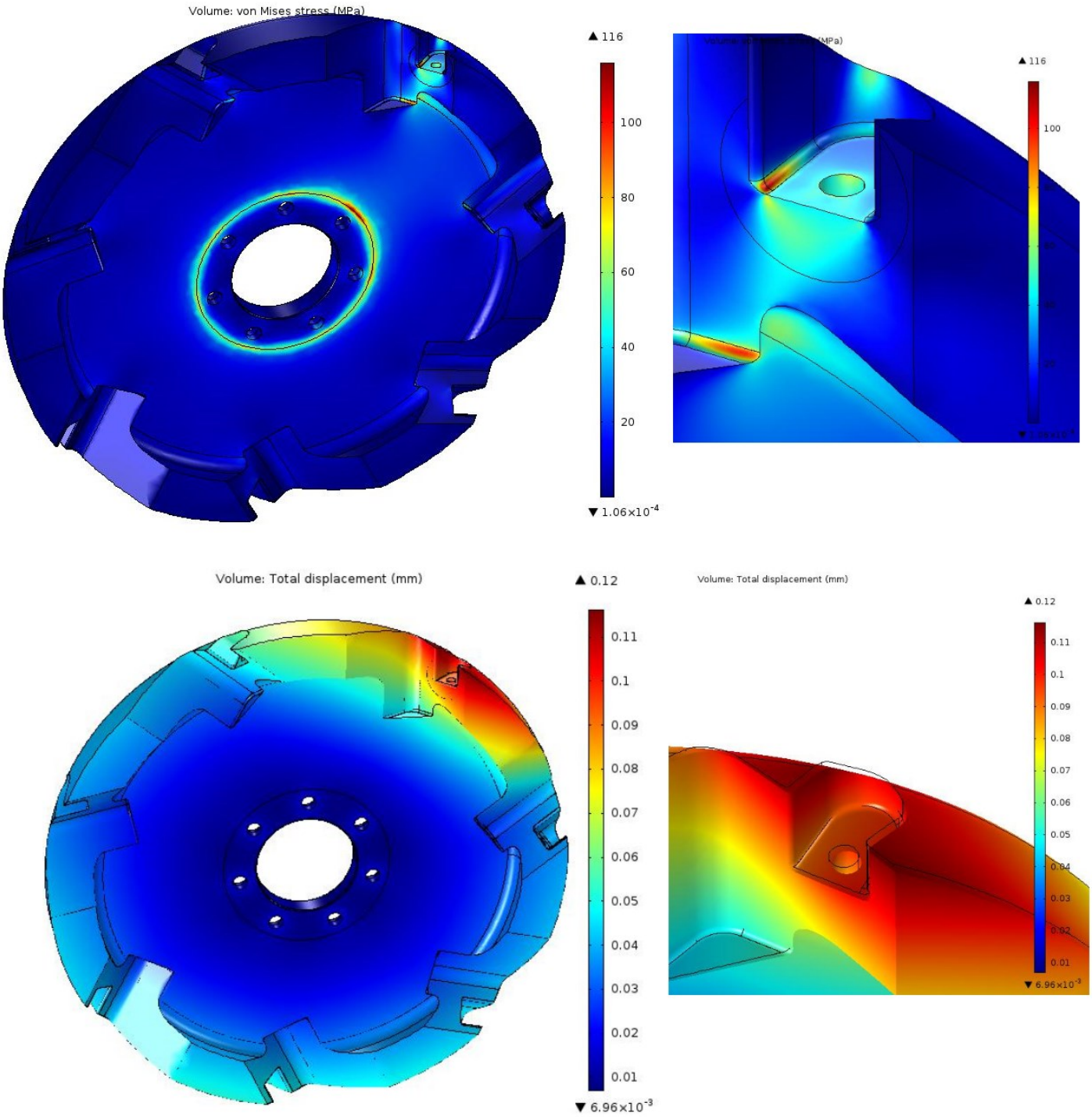

Figure 38. FEA of rims.

A maximum stress of 116MPa in the rims can be observed. The rims are made of aluminum with yielding stress of 235MPa. So the rims are designed with a safety factor of 2. The maximum stress in the material could be reduce by reducing the stress concentration factor on fillet edges. However an increasing of the curvature radius of fillets would imply modification on roller axes geometry and probably an increasing of their complexity and their price.

It can be observed on the previous figure, high stresses on a circle around the connection with the shaft. These stresses are due to defaults in the model and conservative approximations. The area around connection between the shaft and rims has been further studied in a second simulation. The result of this simulation is presented in Figure 39.

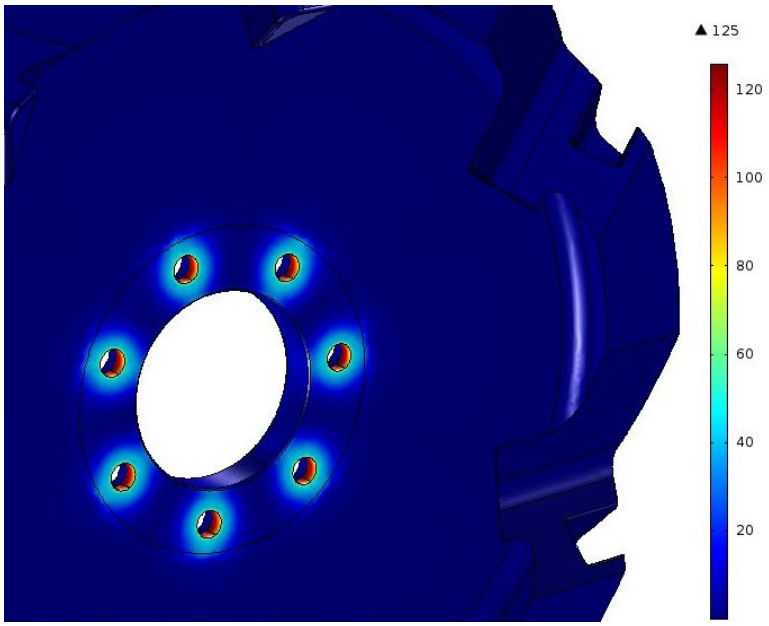

Figure 39. FEA for bolted joints.

A maximum stress of 125MPa has been obtained with this study. This value is a bit higher than the maximum stress observed in the previous study. It could be interesting to increase lightly the thickness of rims in order to have the same maximum stress at the two points. But such decision hasn't been taken since this study still doesn't perfectly describe stresses due to bolted joints.

3.7 Subsystem 4: Shaft

The study of the shaft is composed of a guiding element selection and an analytical analysis on stresses applied on the shaft. The stress analysis was performed using MATLAB.

Guiding elements

The shaft is connected to the support frame through a set of two bearings. Since the wheels rotate with a very low speed compare to the nominal rotating speed of bearings, it has been assumed that the load is static. Roller bearings have then been selected because they have a better resistance to static loads than ball bearings. It can be observed in the structural analysis that bearings are heavily loaded compare to the load applied on the wheel due to the lever arm effect. So in order to reduce this effect tapered roller bearings with O arrangement have been selected. The assembling is presented in Figure 40.

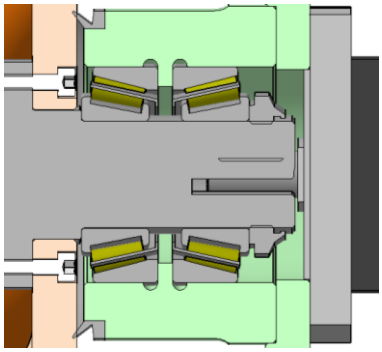

Figure 40. Bearing arrangement.

It could be interesting to select two bearings of different size, to have a smaller and cheaper bearing in the motor side. However it has been determined that the cost saving is greater with same bearings due to size effect on the price than with two different types of bearings.

According to SKF website, bearings must be preload in such way that one bearing compensates the axial force of the other. So the preloading force, F_{rb}, is given by equation(30).

$$F_{rb} = \max\left(\frac{\sqrt{Y'^{2}_{54} + Z'^{2}_{54}}}{2 \cdot Y} - \frac{\sqrt{Y'^{2}_{54} + Z'^{2}_{54}}}{2 \cdot Y} + X_{54}\right) \tag{30}$$

Where Y is a bearing constant equal to 1.7 for selected bearings on SKF website. After calculation, the preloading for is equal to 2 075N. The preloading is realized by a self-locked nut which prevent untightening due to vibrations.

Bearings are lubricated with grease. In fact grease is more adapted than oil for high loads and low speed movements. It also naturally protects bearings from excessive dust. In order to reduce grease replacement and increase bearings' lifetime, bearings access is sealed with a V-ring joint.

Shaft dimensioning

The shaft is making the connection between the rims and the support frame and so it transmits all effort from the motor to the rims. From results of structural analysis, it has been observed that the shaft is subjected to forces and torques in every directions. So in order to keep a good understanding of efforts applied on the shaft as well as constraints that they induce, the dimensioning of the shaft has been realized with an analytical model. All positions of rollers have been studied to describe loading cases of the shaft using α parameter defined in the previous chapters.

Based on the structural analysis, efforts applied on the shaft in every section have been determined. The sections are described using the x coordinate on axis presented in Figure 43.

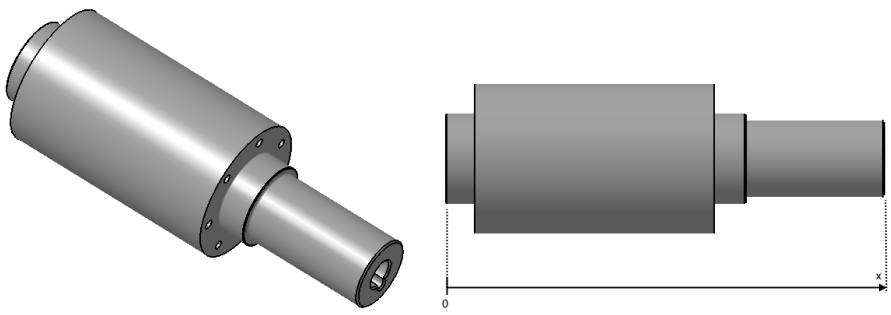

Figure 43. Shaft geometry.

The figure above also shows the geometry of the shaft that have been used to determine Von Mises constraints.

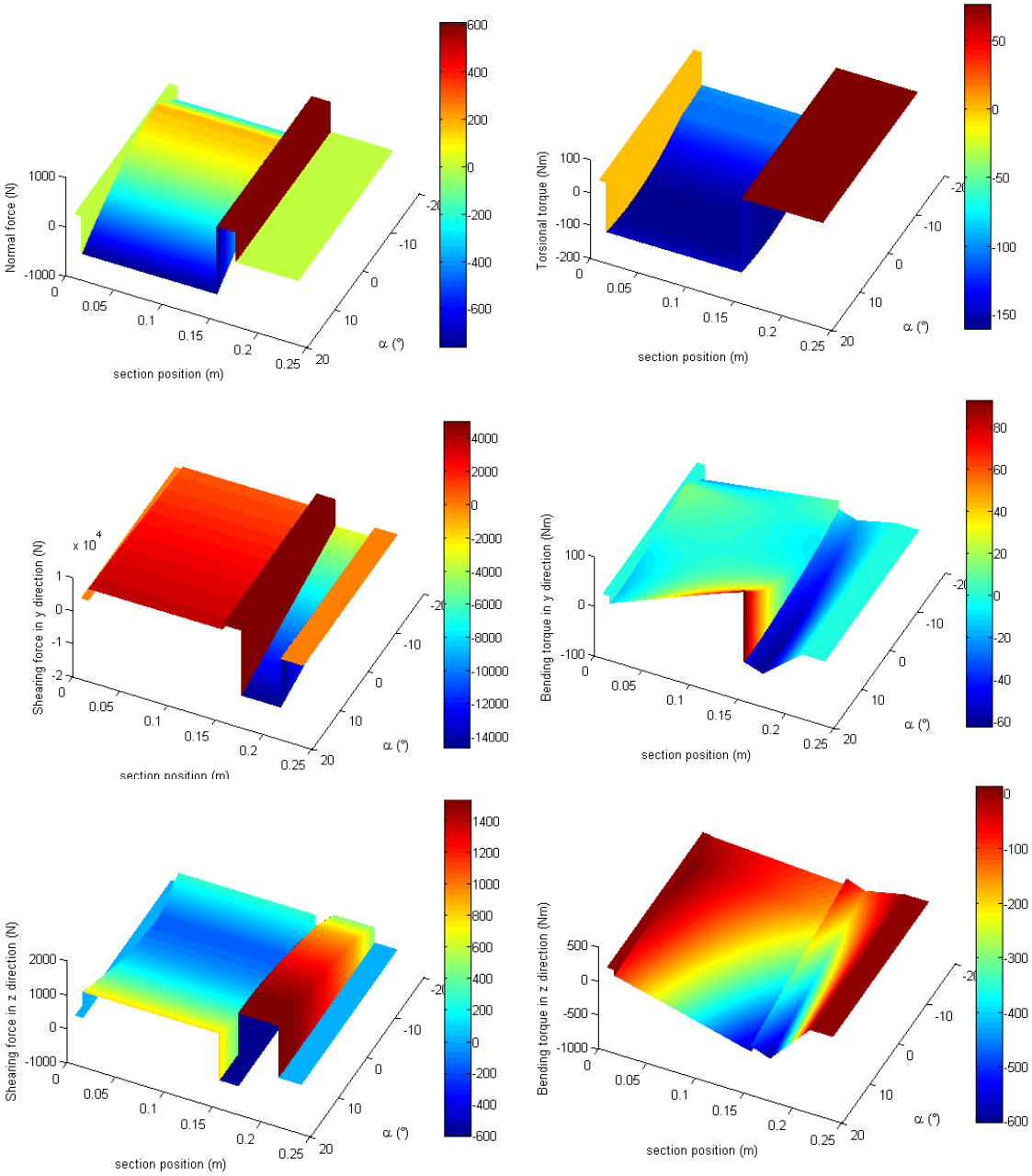

Figure 41. Efforts on shaft sections depending on α in the forward case.

The results for backward case can be observed in Figure 42.

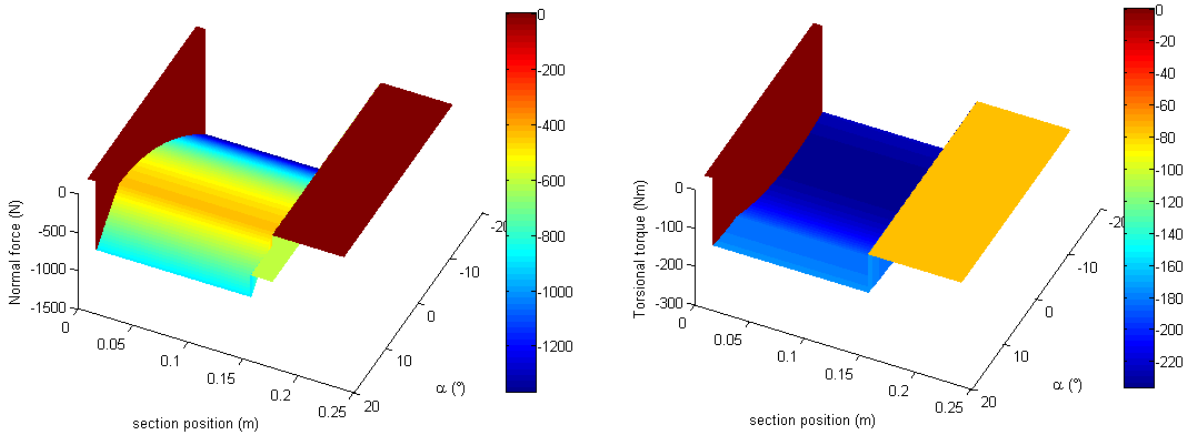

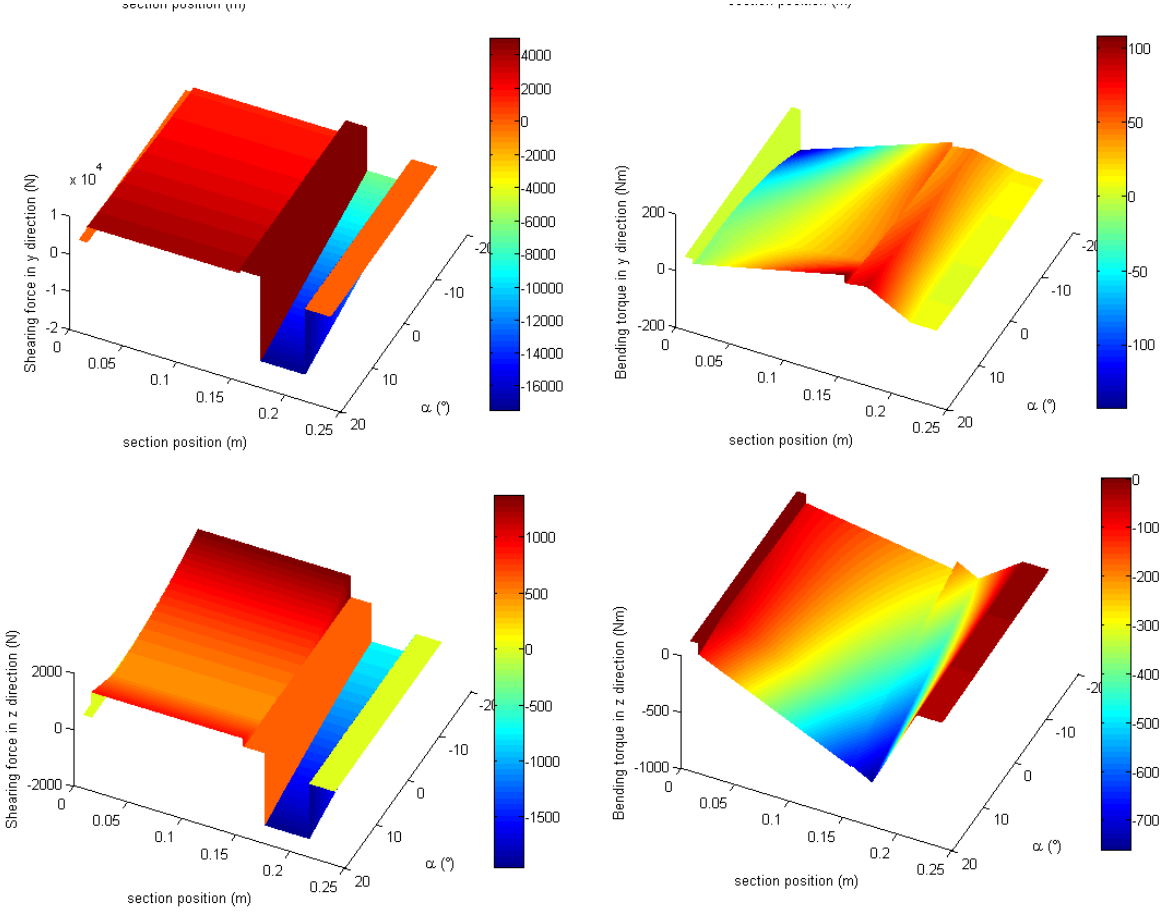

Figure 42. Efforts on shaft sections depending on α in the backward case.

From these figures and with equations(31), the Von Mises constraints in every section of the shaft have been calculated. Only the outer surface of the shaft has been considered in these equations because it's where there is the highest stresses.

$$\sigma = \frac{4N}{\pi \cdot D_s} + \frac{32 \cdot \sqrt{M_{b,y}{}^2 + M_{b,z}{}^2}}{\pi \cdot D_s{}^3} \qquad \tau = \frac{16 \cdot M_t}{\pi \cdot D_s{}^3} \tag{31}$$

Where N is the normal force on the section, $M_{b,y}$ and $M_{b,z}$ are the bending torque in the y and z directions, M_t is the torsional torque and D_s is the diameter of the shaft in the considered section. From the normal stress and the shearing stress calculated in equations (31), the Von Mises constraint has been calculated with equation (32).

$$\sigma_{vm,s} = \sqrt{\sigma^2 + 3 \cdot \tau^2} \tag{32}$$

Based on geometry and efforts applied on each section of the shaft, the maximum Von Mises constraints have been calculated for every loading cases. The results are presented in Figure 44 and 45.

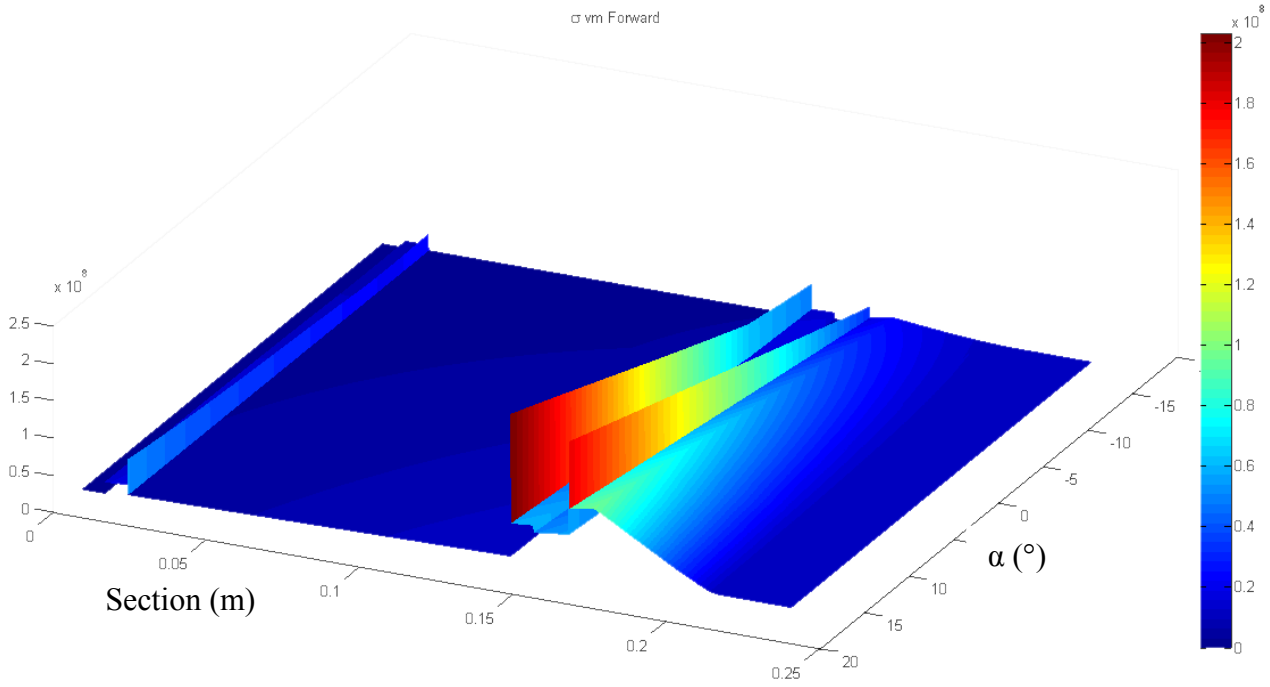

Figure 44. Von Mises stresses in the shaft in the forward case.

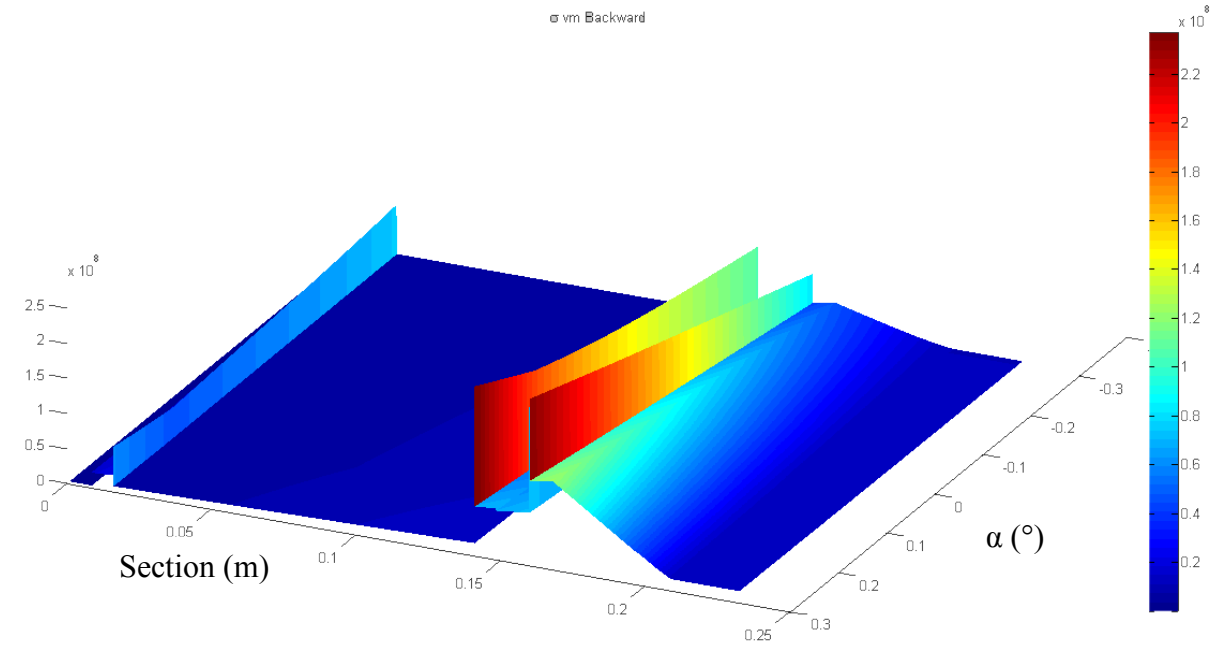

Figure 45. Von Mises stresses in the shaft in the backward case.

Stress concentration factor have been added to the model using the work of Pilkey (2008). It can be observed that a maximum stress of 237MPa appears in the shaft shoulder used to stop the axial movement of bearing. In order to keep the simple geometry of the shaft, methods to reduce the stress concentration haven't been investigated and the aluminum alloy 7075 has been selected as shaft material. This alloy has an elastic limit of 503MPa, so the shaft has been designed with a safety factor of 2.

3.8 Subsystem 5: Support frame

The support frame is making the connection between the bearings and the chassis of the vehicle. This component also plays the role of bearing housing. Due to this function it has been designed to be manufacture with a turning machine. The geometry of the resulting component is presented in Figure 46.

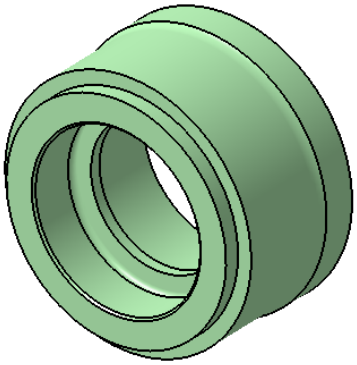

Figure 46. Geometry of the support frame.

Since this component is the last one which has been dimenssioned for the wheel assembly. It hasn't been subjected to major modfications due to other components dimensioning. The dimensioning of the support frame was then realised through an FEA. This method provides a quick and accurate result for this type of geometry. The results obtained with the simulation are shown in Figure 47.

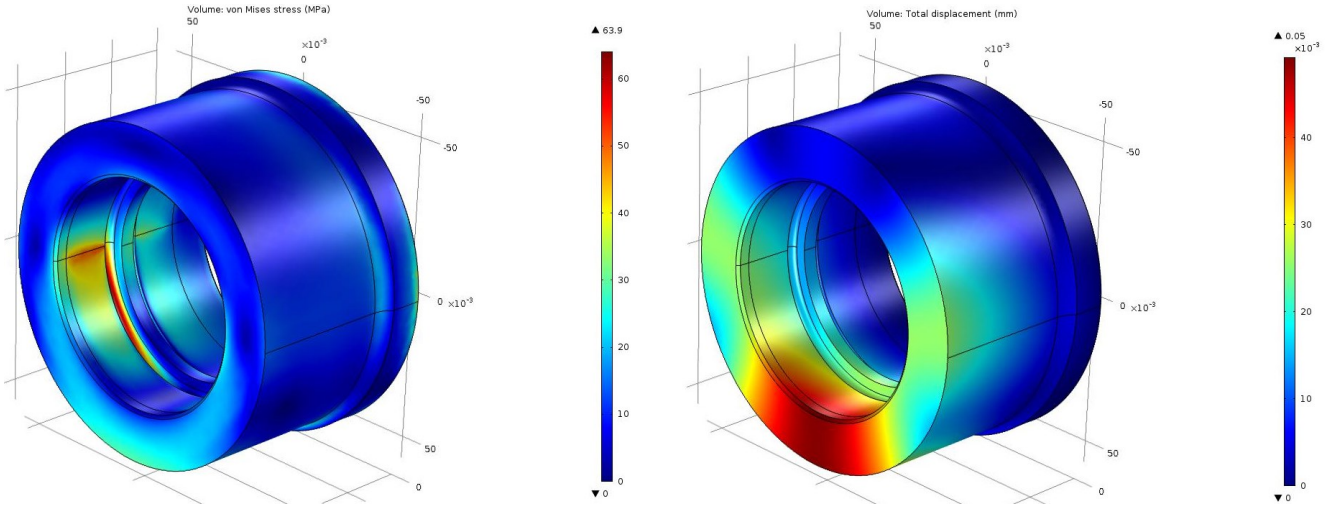

Figure 47. FEA of the support frame.

The support frame is made of aluminum and the maximum stress is equal to 64MPa, so the support frame has been designed with a safety factor of 3.5. The thickness of the support frame could be reduced to cut the price of the component while keeping a safety factor higher or equal to 2. However this thickness has been kept to have a good component stiffness and a maximum deformation of 50µm which provides a good stability to the wheel.

3.9 Chassis dimensioning

The chassis of the vehicle carries a payload of 1 525kg and a load of 150kg coresponding to the weight of batteries. The batteries are seperated in two racks of 75kg each. The payload is distributed on four points on the chassis. These four points enable the customer to fix different adaptators depending on the load that the vehicle is transporting. In fact the vehicle has been designed to transport a pallet but it can be used to transport other types of loads as long as they don't exceed the maximum capacity of the vehicle.

The design of the chassis has been realised with sheets and tubes of steel which are weld together. This solution has been selected because it provides a strong system for a low price specially for the planned batch size of the AGV. The design is presented in Figure 48.

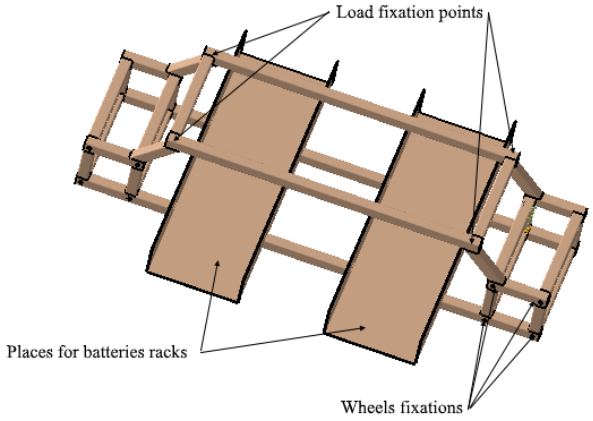

Figure 48. Chassis geometry.

It can be observed on the previous Figure that baterries racks have been placed under the load in order to save some space. The wheels are screwed to the sides of the chassis to offer an easy assembling and an easy maintenance. The loading points are placed at the corners of the structure to reduce its deformation.

A FEA has been realised to validate the resistance of the chassis. With the results from the structural analysis as well as those from the previous part, the following result has been obtained.

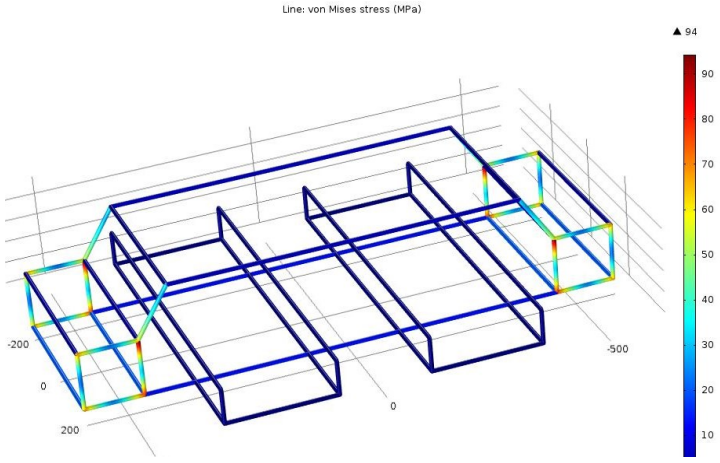

Figure 49. FEA of the chassis.

The steel used for the assembly has an elastic limit of 235MPa so the chassis has been designed with a safety factor of 2.5. This safety factor which is higher than the targeted value has been selected to enable the vehicle to resist to bad loading conditions that may occur during the product lifetime.

Moreover, this version of the chassis is a light one, extra material will probably be added to fit electric and electronical constraint as well as aesthetic constraint. The extra material that is going to be added will increase the stiffness and the resistance of the chassis.

It was noticed that the chassis have a weight of 50kg and so the total mass of the vehicle is around 300kg which is less than the estimation made at the beginning of the study. Since the wheel dimensioning takes into account the weight of the vehicle, this result highlights an overall safety factor applied on wheels.

3.10 Test rigs

The wheels have been tested to validate their performances and all selected technological solutions. The test rigs had to be realised to verified properties with simple solutions based on components and materials already existing within the company. Based on these requirements two test rigs have been designed.

Lifetime test

The first test rig was made to verify the lifetime of components and their wear at 20% of the maximum load. This load corresponds to the load of the vehicle without the mass to transport. The designed solution is presented in Figure 50.

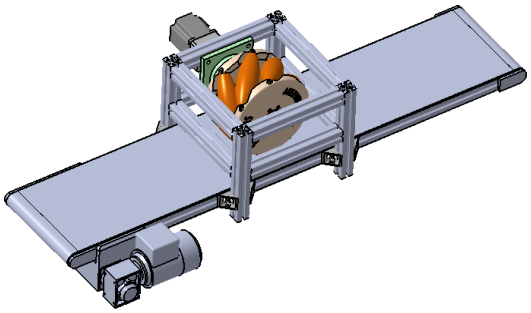

Figure 50. Lifetime test rig.

The test rig is composed of a conveyor and a structure in aluminum profile. The wheel is attached to the structure and positioned on the conveyor. A force corresponding to 102kg is applied on the structure and the structure is screwed to the conveyor in the obtained position. The conveyor is then turned on to simulate the rotation of the wheel on the floor.

Maximum load test

The second test rig was made to verify the maximum load of the wheel in static case. The selected solution is presented in Figure 51.

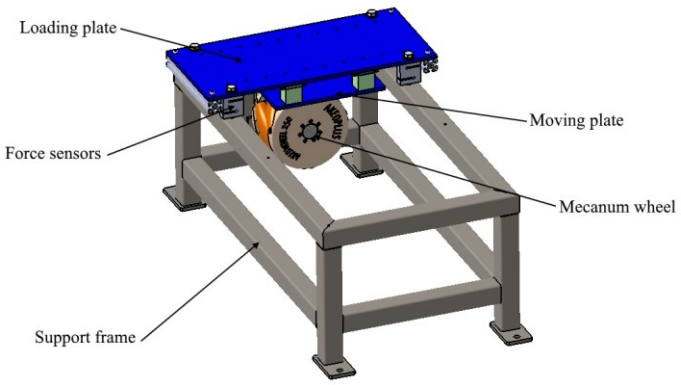

Figure 51. Maximum load test rig.

The test rig is composed of a support frame on which the wheel is attached and two plates, a loading plate and a moving plate. The loading plate is screwed on the support frame. Screws linking the two components are used to load the wheel since these components aren't in contact. Force sensors are placed between the two components to check the loading force applied on the wheel. The force is applied through a moving plate used to slightly rotate the wheel and so check the resistance of the wheel in different positions of the roller in contact.

4 RESULTS

The results of the study are presented in this chapter as well as encountered problems which aren't totally solved in this study.

After consultation of subcontractors of the company, it appears that the new design is 10% cheaper than the one previously realised within the company. Since the first design was realized without any calculation model, this solution also provides a better guarantee that wheels can actually carry the required load.

A prototype of the wheel have been realized for test rigs. Unfortunately the manufacturer haven't been able to manufacture polyurethane rollers. In fact the material is too flexible to be properly machined. So the wheel has been manufactured with PMMA rollers. Since the rollers are the components the most likely to break during the maximum loading test according to the study, this test hasn't been realized for now.

The lifetime test has been performed for 120 hours. It appears that the wear problem of motor shaft is solved with this new design. However abrasive wear appears on rims in the contact surface with the bushing as it can be observed in Figure 52.

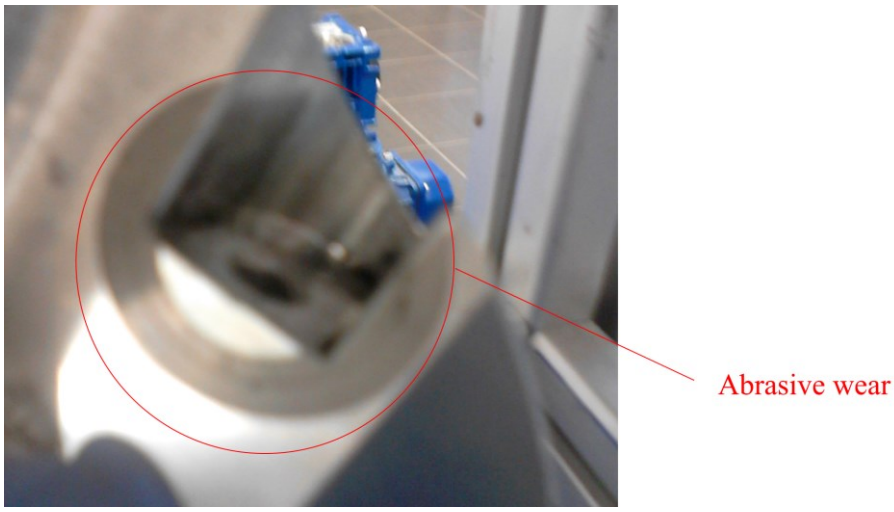

Figure 52. Wear of rims.

5 DISCUSSION AND CONCLUSIONS

The results obtained in this study are discussed in this chapter and conclusions are drawn from the study and its results.

5.1 Discussion

This design corrects some drawbacks of the first design and provides cheaper products. However due to the problems encountered during the manufacturing of rollers, the new design of the wheel haven't been fully tested and approved.

The lifetime test already shows a default in the system that need to be corrected before introduction on the market. Since the bushing is rotating against a hard material which is hardened steel and a soft material which is aluminum at the same time, no obvious materials combination has been find. This problem is then still unsolved for now.

5.2 Conclusions

This study provides a complete methodology to design an AGV including mecanum wheels and the chassis. The methodology has been applied on a practical case but it can easily be employed to develop vehicles with different load capacities and sizes. However a part of the technical solutions that have been selected for the practical case are related to the strategy and possibilities of the company where the thesis has been performed. These solutions need to be reconsidered if this study is used to develop another vehicle.

6 RECOMMENDATIONS AND FUTURE WORK

Recommendations and precautions that need to be considered to design an AGV are presented in this chapter. This recommendations are based on the experience acquired by the author during this study and are meant to provide guidance to someone who would like to realize a similar work. This chapter also includes recommendation for future work that the author would have performed if he had an infinite time to perform the study.

6.1 Recommendations

Based on the study realized, it's recommended to design rollers and manufacture them for tests as soon as possible in this study. In fact, many problems and side effects described in the literature and observed in this study are related to rollers and particularly their geometry and material.

Moreover components of the vehicle are made of material well known and can be modelled with theories extensively used for dimensioning and so they need less attention form the designer.

6.2 Future work

The product developed in this study will be produced in small quantities and so the following points haven't been discussed due to a lack of time and means allocated to the project. Besides, to develop a high-end product with a long lifetime, the following points should be further studied.

- Geometry of rollers
- Modelling of polyurethane behavior during loading
- Fatigue resistance of components
- Manufacturing tolerances of components

7 TABLE OF FIGURES

8 REFERENCES

Intersil group, *"How semiconductors are made"*, http://rel.intersil.com/docs/lexicon/manufacture.html, accessed 2016-02-08, 2010.

Egemin automation, *"History of AGVs: 1953 First AGV"*, http://www.egeminusa.com/pages/agv_education/education_agv_history.html , accessed 2016-02-14, 2001.

Taheri H., Qiao B., Ghaeminezhad N., *"Kinematics model of a four mecanum wheeled mobile robot"*, International Journal of Computer Applications, Vol. 113, No. 3, 2015.

European Pallet Association E.V., *"EPAL Euro pallet"*, http://www.epal-pallets.org/uk/downloads/Product%20specification%20sheet%20EPAL%20Euro%20pallet%2005-16.pdf, accessed 2016-07-18, 2016-05.

Diegel O., Badve A., Bright G., Potgieter J., Tlale S., *"Improved Mecanum wheel design for Omni-directional Robots",* Australasian Conference on Robotics and Automation, Auckland, 2002-11-27.

De Villiers M., Tlale N., *"Kinematics and Dynamics Modelling of a Mecanum Wheeled Mobile Platform",* Mechatronics and Machine Vision in Practice, 2008.

Matsinos E., *"Modelling of the motion of a Mecanum-wheeled vehicle"*, 2012-11-10.

Ilon B.E., *"Wheels for a course stable self-propelling vehicle movable in any desired direction on the ground or some other base»*, US Patent US 3876255 A, 1972-11-13

Potter S. D., *"Omni-directional wheel"*, US Patent US 2010/0187779 A1, 2009-01-26.

Zdrahal P., Uebelhart B., Spindler Z., *"Mecanum Wheel and Mecanum-wheeled Vehicle"*, US Patent US 2014/0232174 A1, 2014-08-21.

Gfrerrer A., *"Geometry and Kinematics of the Mecanum Wheel"*, Computer Aided Geometric Design, Vol. 25, p.784-791, 2008-07-08.

Cambridge University Engineering Department, *"Materials Data Book",* 2003.

Bae J-J., Kang N., *"Design Optimization of a Mecanum Wheel to Reduce Vertical Vibrations by the Consideration of Equivalent Stiffness",* Shock and Vibration, Vol. 2016, 2016-02-14.

Guenther, *"Wheel",* CN Patent CN 101223039 A, 2008-07-16.

Juvinall R.C., Marshek K.M., *"Fundamentals of Machine Component Design"*, Fourth Ed. , John Wiley & Sons Pte Ltd, Hoboken, New Jersey, 2006.

Kauzlarich J.J., Thacker J.G., *"Wheelchair tire rolling resistance and fatigue"*, Journal of Rehabilitation Research and Development, Vol. 22, No. 3, p.25-41, 1985.

Qi H.J., Boyce M.C., *"Stress-Strain Behavior of Thermoplastic Polyurethane",* Mechanics of Materials, Vol. 37, p. 817-839, 2005-08.

Basf, *"Elastomères de polyurethane thermoplastique",* (FRENCH), 2014.

Inglebert G., Da Silva Botelho T., Lemaire Caron I., *"Théorie du contact de Hertz",* (FRENCH), Techniques de l'ingénieur, TRI200 v1, 2011-09-10.

SKF, *"Determining preload force",* http://www.skf.com/uk/products/bearings-units-housings/ball-bearings/principles/application-of-bearings/bearing-preload/determining-preload-force/index.html, accessed 2016-08-13.

Sunray Inc, *"Understanding Polyurethane Coefficient of Friction"*, Polyurethane products, http://fr.slideshare.net/SunrayInc/understanding-polyurethane-coefficient-of-friction, accessed 2016-03-16, 2013-10-23.

Hamilton G.M., GOODMAN L.E. *"The stress field created by a circular sliding contact"*, Journal of applied Mechanics, p. 371-376, 1966-06.

Pilkey W.D., Pilkey D.F., Peterson's Stress Concentration Factors, 3rd Edition, 2008-02.

APPENDIX A: MECHANICAL TORSORS

This appendix presents the basic notations and properties of mechanical torsors. Since torsors provide simple and efficient descriptions of three-dimensional mechanical problems, they have been extensively used in this study.

Notations

A mechanical torsor is a notation which summarize all mechanical actions between two solids. The mechanical actions of the body 1 applied on the body 2 are then written down:

$$\{\tau(1 \to 2)\}$$

This notation can be decomposed at a specific point in a specific coordinate system in order to get more informations on mechanical actions between the two bodies. The following notation is then used:

$$\{\tau(1 \to 2)\} = \begin{Bmatrix} X_{12} & L_{12} \\ Y_{12} & M_{12} \\ Z_{12} & N_{12} \end{Bmatrix}_{(A,x,y,z)}$$

Where X_{12}, Y_{12}, and Z_{12} are forces applied on the body 2 by the body 1 in the respective directions x, y and z and L_{12}, M_{12} and N_{12} are the moments at the point A in the respective directions x, y and z.

A mechanical torsor can be describe with other notations, but this appendix only presents the ones that have been used in this study.

Formulas to change the coordinate system and to change the application point

Considering two coordinate systems (x, y, z) and (x_1, y_1, z_1) with a common direction z and z_1 and with angle θ between x and x_1. The two coordinate systems are presented in Figure 1.

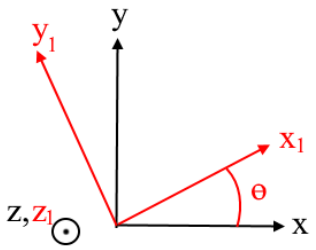

Figure 1. Changing of coordinate systems.

For the mechanical torsor presented above, the formula to change the coordinate system is:

$$\begin{Bmatrix} X_{12} & L_{12} \\ Y_{12} & M_{12} \\ Z_{12} & N_{12} \end{Bmatrix}_{(A,x,y,z)} = \begin{Bmatrix} X_{12}\cdot\cos(\theta)+Y_{12}\cdot\sin(\theta) & L_{12}\cdot\cos(\theta)+M_{12}\cdot\sin(\theta) \\ Y_{12}\cdot\cos(\theta)-X_{12}\cdot\sin(\theta) & M_{12}\cdot\cos(\theta)-L_{12}\cdot\sin(\theta) \\ Z_{12} & N_{12} \end{Bmatrix}_{(A,x_1,y_1,z_1)}$$

Considering two points A and B such as $\overrightarrow{AB} = a \cdot \vec{x} + b \cdot \vec{y} + c \cdot \vec{z}$ and the mechanical torsor introduced in Notations, the formula to change the application point is:

$$\begin{Bmatrix} X_{12} & L_{12} \\ Y_{12} & M_{12} \\ Z_{12} & N_{12} \end{Bmatrix}_{(A,x,y,z)} = \begin{Bmatrix} X_{12} & L_{12} + c \cdot Y_{12} - b \cdot Z_{12} \\ Y_{12} & M_{12} + a \cdot Z_{12} - c \cdot X_{12} \\ Z_{12} & N_{12} + b \cdot X_{12} - a \cdot Y_{12} \end{Bmatrix}_{(B,x,y,z)}$$

Fundamental equations

Since mechanical torsors are simplified notations of mechanical actions, the fundamental equations are still available. Such as the third law of Newton.

$$\{\tau(1 \to 2)\} = -\{\tau(2 \to 1)\} \Leftrightarrow \begin{Bmatrix} X_{12} & L_{12} \\ Y_{12} & M_{12} \\ Z_{12} & N_{12} \end{Bmatrix}_{(A,x,y,z)} = \begin{Bmatrix} -X_{21} & -L_{21} \\ -Y_{21} & -M_{21} \\ -Z_{21} & -N_{21} \end{Bmatrix}_{(A,x,y,z)}$$

Or the static equilibrium of a solid body

$$\{\tau(1 \to 2)\} + \{\tau(3 \to 2)\} + \{\tau(4 \to 2)\} + ... + \{\tau(\mathrm{n} \to 2)\} = \{0\}$$

Which is developed with the following form

$$\begin{Bmatrix} X_{12} + X_{32} + X_{42} + ... + X_{n2} = 0 \\ Y_{12} + Y_{32} + Y_{42} + ... + Y_{n2} = 0 \\ Z_{12} + Z_{32} + Z_{42} + ... + Z_{n2} = 0 \\ L_{12} + L_{32} + L_{42} + ... + L_{n2} = 0 \\ M_{12} + M_{32} + M_{42} + ... + M_{n2} = 0 \\ N_{12} + N_{32} + N_{42} + ... + N_{n2} = 0 \end{Bmatrix}$$

However, it's important to keep in mind that these equations can only be used with torsors which are defined at the same point and in the same coordinate system.

APPENDIX B:STRUCTURAL ANALYSIS EQUATIONS

This appendix presents equations obtained during the structural analysis. Since the geometry of mecanum wheels is quite complex, these equations are also complex and may be of interest only for readers who plan to design mecanum wheels.

It's reminded to the reader that a number have been allocated to each subsystem with the following association

1. Rollers
2. Front rim
3. Back rim
4. Shaft
5. Support frame

The contact point between the considered roller and floor is defined with the angle α. All forces and moments are calculated depending on α to observe their variations during wheel rotation.

The geometry of the wheel with relevant parameters and points is presented in Figure 1.

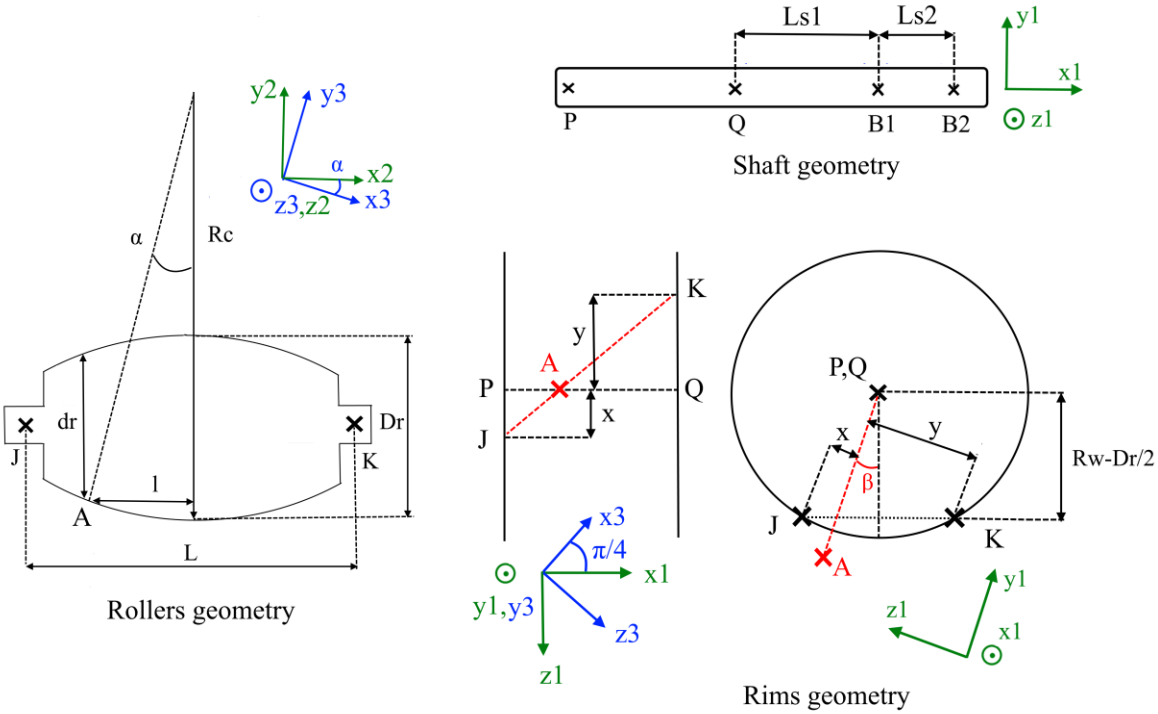

Figure 1. Wheel geometry.

In order to simplify equations, the following geometrical parameters are introduced.

$$l = Rc \cdot \sin(\alpha)$$

$$\beta = \sin^{-1}\left(\frac{l \cdot \sqrt{2}}{2Rw}\right)$$

$$dr = Dr - 2 \cdot Rc\left(1 - \cos(\alpha)\right)$$

$$x = \frac{\sqrt{2}}{2} \cdot \left(\frac{L - 2l}{2} \cdot \cos(\alpha) + \frac{dr}{2}\sin(\alpha)\right)$$

$$y = \frac{\sqrt{2}}{2} \cdot \left(\frac{L + 2l}{2} \cdot \cos(\alpha) - \frac{dr}{2}\sin(\alpha)\right)$$

The vectors below are used to change application points of torsors and so to solve equations.

$$\overrightarrow{JP} = -x \cdot \overrightarrow{z1} + \frac{\text{Rw} - \text{Dr}/2}{\cos(\beta)} + x \cdot \tan(\beta) \cdot \overrightarrow{y1} \qquad \overrightarrow{JK} = L \cdot \overrightarrow{x2} \qquad \overrightarrow{B1Q} = -Ls1 \cdot \overrightarrow{x1}$$

$$\overrightarrow{KQ} = y \cdot \overrightarrow{z1} + \frac{\text{Rw} - \text{Dr}/2}{\cos(\beta)} - y \cdot \tan(\beta) \cdot \overrightarrow{y1} \qquad \overrightarrow{PQ} = \frac{1}{2} L \cdot \overrightarrow{x1} \qquad \overrightarrow{B2Q} = -(Ls1 + Ls2) \cdot \overrightarrow{x1}$$

Equations of rollers

The mechanical actions of rims on rollers are modelled by the following torsors.

$$\{\tau(2 \to 1)\} = \begin{Bmatrix} X_{21} & 0 \\ Y_{21} & 0 \\ 0 & 0 \end{Bmatrix}_{(\text{J,x2,y2,z2})} \qquad \{\tau(3 \to 1)\} = \begin{Bmatrix} X_{31} & 0 \\ Y_{31} & 0 \\ 0 & 0 \end{Bmatrix}_{(\text{K,x2,y2,z2})}$$

And the associated equations are shown below.

$$X_{21} = \left(Ff \cdot \cos(\alpha) + Fr \cdot \sin(\alpha)\right) \cdot \frac{1 - sign(Ff \cdot \cos(\alpha) + \text{Fr} \cdot \sin(\alpha))}{2}$$

$$Y_{21} = \frac{dr}{2L}\left(Fr \cdot \sin(\alpha) + Ff.\cos(\alpha)\right) - \frac{L + 2l}{2L}\left(Fr \cdot \cos(\alpha) - Ff \cdot \sin(\alpha)\right)$$

$$X_{31} = -\left(Ff \cdot \cos(\alpha) + Fr \cdot \sin(\alpha)\right) \cdot \frac{1 + sign(Ff \cdot \cos(\alpha) + \text{Fr} \cdot \sin(\alpha))}{2}$$

$$Y_{31} = -\frac{dr}{2L}\left(Fr \cdot \sin(\alpha) + Ff.\cos(\alpha)\right) - \frac{L - 2l}{2L}\left(Fr \cdot \cos(\alpha) - Ff \cdot \sin(\alpha)\right)$$

Equations of rims

The mechanical actions of shaft on rims are modelled by the following torsors.

$$\{\tau(4 \to 2)\} = \begin{Bmatrix} X_{42} & L_{42} \\ Y_{42} & M_{42} \\ Z_{42} & N_{42} \end{Bmatrix}_{(\text{P,x1,y1,z1})} \qquad \{\tau(4 \to 3)\} = \begin{Bmatrix} X_{43} & L_{43} \\ Y_{43} & M_{43} \\ Z_{43} & N_{43} \end{Bmatrix}_{(\text{Q,x1,y1,z1})}$$

And the corresponding equations are presented below.

$$X_{42} = \frac{\sqrt{2}}{2}\left(X_{21} \cdot \cos(\alpha) - Y_{21} \cdot \sin(\alpha)\right)$$

$$Y_{42} = X_{21} \cdot \sin(\alpha) + Y_{21} \cdot \cos(\alpha)$$

$$Z_{42} = \frac{\sqrt{2}}{2}\left(Y_{21} \cdot \sin(\alpha) - X_{21} \cdot \cos(\alpha)\right)$$

$$L_{42} = \frac{\sqrt{2}}{2}\left(\frac{Rw - Dr/2}{\cos(\beta)} + x \cdot \tan(\beta)\right)\left(X_{21} \cdot \cos(\alpha) - Y_{21} \cdot \sin(\alpha)\right) - x\left(Y_{21} \cdot \cos(\alpha) + X_{21} \cdot \sin(\alpha)\right)$$

$$M_{42} = \frac{\sqrt{2}}{2} x\left(X_{21} \cdot \cos(\alpha) - Y_{21} \cdot \sin(\alpha)\right)$$

$$N_{42} = \frac{\sqrt{2}}{2}\left(\frac{Rw - Dr/2}{\cos(\beta)} + x \cdot \tan(\beta)\right)\left(X_{21} \cdot \cos(\alpha) - Y_{21} \cdot \sin(\alpha)\right)$$

$$X_{43} = \frac{\sqrt{2}}{2}\left(X_{31}\cdot\cos(\alpha) - Y_{31}\cdot\sin(\alpha)\right)$$

$$Y_{43} = X_{31}\cdot\sin(\alpha) + Y_{31}\cdot\cos(\alpha)$$

$$Z_{43} = \frac{\sqrt{2}}{2}\left(Y_{31}\cdot\sin(\alpha) - X_{31}\cdot\cos(\alpha)\right)$$

$$L_{43} = \frac{\sqrt{2}}{2}\left(\frac{Rw - Dr/2}{\cos(\beta)} - y\cdot\tan(\beta)\right)\left(X_{31}\cdot\cos(\alpha) - Y_{31}\cdot\sin(\alpha)\right) + y\left(Y_{31}\cdot\cos(\alpha) + X_{31}\cdot\sin(\alpha)\right)$$

$$M_{43} = \frac{\sqrt{2}}{2}y\left(Y_{31}\cdot\sin(\alpha) - X_{31}\cdot\cos(\alpha)\right)$$

$$N_{43} = \frac{\sqrt{2}}{2}\left(\frac{Rw - Dr/2}{\cos(\beta)} - y\cdot\tan(\beta)\right)\left(X_{31}\cdot\cos(\alpha) - Y_{31}\cdot\sin(\alpha)\right)$$

Equations of shaft

The mechanical actions of the support frame on the shaft are modelled by the following torsors.

$$\{\tau(5\to 4)\} = \begin{Bmatrix} X_{54} & 0 \\ Y_{54} & 0 \\ Z_{54} & 0 \end{Bmatrix}_{(B1,x1,y1,z1)} \qquad \{\tau'(5\to 4)\} = \begin{Bmatrix} 0 & 0 \\ Y'_{54} & 0 \\ Z'_{54} & 0 \end{Bmatrix}_{(B2,x1,y1,z1)}$$

And the corresponding equations are presented below.

$$X_{54} = X_{42} + X_{43}$$

$$Y_{54} = \frac{-N_{42} - N_{43} + Y_{42}\cdot L\cdot\frac{\sqrt{2}}{2} + \left(Ls1 + Ls2\right)\cdot(Y_{42} + Y_{43})}{Ls2}$$

$$Z_{54} = \frac{M_{42} + M_{43} + Z_{42}\cdot L\cdot\frac{\sqrt{2}}{2} + \left(Ls1 + Ls2\right)\cdot(Z_{42} + Z_{43})}{Ls2}$$

$$Y'_{54} = \frac{N_{42} + N_{43} - Y_{42}\cdot L\cdot\frac{\sqrt{2}}{2} - Ls1\cdot(Y_{42} + Y_{43})}{Ls2}$$

$$Z'_{54} = \frac{-M_{42} - M_{43} - Z_{42}\cdot L\cdot\frac{\sqrt{2}}{2} - Ls1\cdot(Z_{42} + Z_{43})}{Ls2}$$